ChemCatChem

Research Article
doi.org/10.1002/cctc.202400613

Chemistry Europe
European Chemical Societies Publishing

www.chemcatchem.org

Improving the Ca-assisted Urea-Glass Method for the Synthesis of Zirconium Nitride as Potential Electrocatalyst for the Nitrogen Reduction Reaction

Sebastian C. H. Bragulla,*[a, c] Aaron R. von Seggern,[a, d] Julian Lorenz,[a] Corinna Harms,[a] Michael Wark,[d] and K. Andreas Friedrich*[b, c]

Zirconium mononitride (ZrN), among other nitrides, is of interest as a catalyst in general and especially for the electrochemical nitrogen reduction reaction (NRR). Synthesis of nanoparticulate ZrN is challenging due to the formation of undesired other phases and the need for hazardous precursors or high temperatures. The urea glass method (UGM) was used in this work to synthesise nanoparticulate zirconium nitride. A focused parameter variation of the precursor composition and process conditions lead to an optimised synthesis, greatly improving material purity in regard to minor phase and residual carbon content. The nitride starts to form at a pyrolysis temperature of 900 °C, likely by irreversible decomposition of previously-formed oxynitride, which forms from amorphous ZrO_2 and urea during pyrolysis. An increased pyrolysis temperature improves product purity but slightly lowers nitride purity. Calcium admixture slows the urea decomposition, yielding a more phase-pure product with less residual carbon at low amounts. A classical carbothermal nitridation (CN) was used in comparison to the UGM to synthesise ZrN. This was successful in synthesising zirconium carbonitride Zr(N, C) without minor phase, but significant carbon remains if added overstoichiometrically. Using less carbon and a longer dwelling time yielded ZrN without significant carbide (ZrC) incorporation or residual carbon, but with some minor ZrO_2 phase, proving a promising synthesis route. A limited electrochemical investigation of a synthesised ZrN material was carried out to scope the general material behaviour and to qualitatively derive the potential catalytic activity for the NRR. Higher reductive currents in nitrogen-saturated electrolyte qualitatively point to NRR activity, but further and more in-depth examination is required.

1. Introduction

Catalysts are indispensable for today's society and industry. They enable efficient, selective and high-yield economical production of a plethora of products. The industrial scale production of ammonia via the Haber-Bosch process using an iron catalyst is a famous example, with an estimated world-wide production of 150 Mt in 2021.[1,2] Many catalyst materials are made from noble metals because of their beneficial material properties. Transition metal carbides (TMC) and transition metal nitrides (TMN) have similar electronic properties as noble metals, making them promising alternative catalyst materials to rare noble metals. TMNs are of interest as catalysts for several electrochemical reactions such as hydrogen evolution reaction (HER), oxygen evolution reaction (OER) and more.[3,4] Furthermore, TMNs are of special interest for the electrochemical nitrogen reduction reaction (NRR), which potentially can enable a small-scale on-demand electrochemical ammonia synthesis (EAS) directly from water, nitrogen and renewable electricity. To date, EAS suffers from insufficiently active and selective catalysts, resulting in production rates and efficiencies more than one order of magnitude too small for commercialisation.[5] Most of these catalyst materials are fundamentally limited by their reaction mechanism.[6] Certain TMNs are promising alternatives, because they catalyse the NRR via a Mars-van-Krevelen mechanism, possibly circumventing these limitations.[7] Zirconium nitride (ZrN) is one of the promising candidates. Theoretical investigations have identified the cubic (100) facet of ZrN as active, selective and stable for NRR.[7] Recent experimental investigation of sputtered ZrN thin films showed ammonia production, but limited surface area and solubility of nitrogen in the electrolyte were barriers to a proof of genuine NRR activity.[8] For this reason, investigating nanoparticulate ZrN as an electrocatalyst for NRR is highly interesting. However, synthesising TMN nanoparticles with the desired properties is complex. ZrN can be synthesised by a variety of physical and

[a] S. C. H. Bragulla, A. R. von Seggern, J. Lorenz, C. Harms
Institute of Engineering Thermodynamics, German Aerospace Center (DLR), Carl-von Ossietzky-Str. 15, Oldenburg 26129, Germany
E-mail: Sebastian.Bragulla@dlr.de

[b] K. A. Friedrich
Institute of Engineering Thermodynamics, German Aerospace Center (DLR), Pfaffenwaldring 38–40, Stuttgart 70569, Germany
E-mail: Andreas.Friedrich@dlr.de

[c] S. C. H. Bragulla, K. A. Friedrich
Institute for Building Energetics, Thermotechnology and Energy Storage (IGTE), University of Stuttgart, Pfaffenwaldring 31, Stuttgart 70596, Germany

[d] A. R. von Seggern, M. Wark
Institute of Chemistry, Chemical Technology 1, Carl von Ossietzky University Oldenburg, Carl-von-Ossietzky-Str. 9–11, Oldenburg 26129, Germany

Supporting information for this article is available on the WWW under https://doi.org/10.1002/cctc.202400613Supporting information for this article is available on the WWW under https://doi.org/10.1002/cctc.202400613

chemical processes, such as physical or chemical vapour deposition (PVD or CVD), direct nitridation of the metal or oxide, ammonolysis of zirconium halides or carbothermal nitridation.[9–12] Lerch et al. synthesised Zr_3N_4 by reaction of $ZrCl_4$ with NH_3 at 850–950 °C, which decomposes to high-purity ZrN at 800 °C.[9] Parkinson and Nelson synthesised ZrN by carbothermic reduction nitridation from ZrO_2 and graphite at temperatures of 1400–2000 °C.[13] These methods require either special equipment (PVD, CVD), hazardous precursors (metallic Zr, NH_3) or high temperatures (>1400 °C). The achievable nitride purity, phase purity (minor phases) and material purity (residual carbon) vary depending on the synthesis method. Instead, urea has been used as cheap, non-toxic, easy-to-handle *in situ* nitrogen source to synthesise different TMN nanoparticles by a non-aqueous sol-gel route at moderate temperatures.[14] This route, termed 'urea-glass method' (UGM) by Giordano et al., is accessible, versatile and easy to adapt.[14] A variety of TMNs were successfully synthesised by UGM, for example chromium and vanadium nitride.[14] However, precise control of the occurring phases (oxide, oxynitride, nitride, carbide) and their purity, as well as the overall sample composition (residual carbon) is complex, because the reactive atmosphere is generated *in situ* and is not under direct process control. Gao et al. developed the Ca-assisted UGM by adding calcium ions, which slows the urea decomposition down. This slowed-down urea decomposition allows for more control over the occurring nitride phases and enabled synthesis of the desired tantalum nitride phase. A small calcium admixture also resulted in more homogeneous and phase pure nitride nanoparticles. Larger calcium admixture resulted in the formation of oxynitrides. An additional advantage of the calcium admixture was the reduction of remaining residual carbon from the decomposition of urea during pyrolysis.[15] Investigating these effects of a calcium admixture to optimise the synthesis of zirconium nitride by UGM is attractive to achieve synthesis of high-purity zirconium nanoparticles for use as electrocatalyst.

In this study, we aimed to synthesise nanoparticulate ZrN as prospective electrocatalyst material using the UGM as accessible and versatile synthesis route. In doing so, we varied the pyrolysis mixture (urea content, calcium admixture), pyrolysis temperature and dwelling time to achieve, in order, an ideally pure nitride phase, minimal minor phases, homogeneous nanoparticles, and minimal residual carbon in the synthesis product. In addition, we also employed a classical carbothermal nitridation (CN) at high temperature as alternative method for synthesizing zirconium nitride in a limited capacity, to illustrate the use of both methods in comparison. The synthesised powders were structurally studied by various physical characterisation techniques to investigate the effect of the parameter variations. A limited electrochemical investigation of synthesised materials in regard to their electrocatalytic behaviour for the NRR will also be presented.

2. Results

An overview of all samples synthesised can be found in the supporting information Table S1. The samples have been numbered consecutively with Roman numerals (I–XXV) for cross-reference. These numbers are stated in the labels of graphs to reference samples i.e. indicate one and the same sample shown in more than one graph.

The following section starts with an overview of X-ray diffraction (XRD) patterns of relevant zirconium phases taken from literature and used for reference. This is followed by a short description of the sol-gel synthesis as starting point of the synthesis. The impact of the varied parameters, namely pyrolysis temperature and calcium admixture, on the occurring phases are discussed thereafter as initial main focus of this work. The effect of a lower urea content and the impact of the choice of pyrolysis vessel are discussed in the supporting information. These results are concluded with a comparison of the urea-glass method with the high-temperature synthesis of zirconium nitride by carbothermal nitridation. Further characterization of the UGM samples by X-ray photoelectron spectroscopy (XPS) and transmission electron microscopy (TEM) is presented at the end. The results close a with limited electrochemical investigation.

2.1. Ceramic Phases of Zirconium – Nitride, Oxynitride and Oxide

There is some uncertainty in the exact value of the lattice constant of zirconium nitride and zirconium carbide. Both materials are easily contaminated by carbon and nitrogen respectively, as well as oxygen. This contamination affects the measured lattice constant to a different degree. Subsequently, there is some variation in the given lattice constant for these 'pure' compounds depending on the literature source. Most reliable are literature sources in which an accompanying elemental analysis was carried out. An overview of the major XRD patterns of relevant zirconium nitride, oxynitride and oxide phases we used for reference in this work are shown in the supporting information (Figure S1). The ICDD Powder Diffraction File (PDF) card and associated literature source of these XRD patterns are given in Table 1 below. In general, PDF patterns with available cited literature were chosen. The works

Table 1. Reference X-ray diffraction (XRD) patterns of zirconium nitride, oxynitride, and oxide used in this work.

Phase	ICDD PDF	Literature
$ZrN_{0.97(4)}$	–	[16]
ZrN	98-064-4895	[17]
γ (Zr_2ON_2)	98-008-8666	[18]
β ($Zr_7O_8N_4$)	98-024-5751	[19]
β′ ($Zr_7O_{11}N_2$)	98-015-7959	[20]
m-ZrO_2	98-005-7158	[21]
t-ZrO_2	98-008-5322	[22]

of Lerch et al. and Constant et al. were selected, because both give accompanying chemical compositions for the investigated compounds.[16,17] Moreover, Constant et al. specifically investigated the change in lattice constant of solid-solutions of zirconium nitride and zirconium carbide.[17] The data given by Constant et al. for zirconium mononitride (ZrN) and zirconium carbide (ZrC) was used below to calculate the stoichiometries of selected synthesised samples by Vegard's Law (SI S13).[17]

The different oxynitride phases, β, β′ and γ, differ in nitrogen and oxygen content and are difficult to distinguish by PXRD, as can be seen in Figure S1b. This difficulty in assigning phases is further compounded by the position of the main peak of tetragonal zirconium dioxide (t-ZrO_2). These circumstances often prevent unequivocally assigning a pattern to an occurring low intensity minor phase. Semiquantitative evaluation of phases by their intensity as available in the used HighScore + software version 4.1 with PDF4 database (2014) was thus not used for this reason. For the sake of transparency and comparability, all diffractograms show as-recorded data without any background correction. The diffractograms have been scaled to the highest intensity peak if not specified differently. All angles given in this work refer to 2θ angles.

2.2. Sol-Gel Synthesis

The sol-gel synthesis yielding the pyrolysis mixture directly affects the synthesis of the desired nitride. Dried ethanol absolute was used as non-toxic, readily available solvent for the sol-gel synthesis.[23] Zirconium tetrachloride reacts with ethanol to form an alkoxide.[14] However, this reaction is incomplete. A hydrogen chloride acceptor such as ammonia can be used to complete the reaction.[24] The incompletely reacted zirconium tetrachloride proved to be more stable against unwanted, premature hydrolysis and polycondensation by traces of moisture than commercial zirconium ethoxide. A 28 wt.% ammonium hydroxide solution was used in this work for the purpose of completing the reaction of the zirconium tetrachloride to the ethoxide, which caused the reaction to be accompanied by rapid crosslinking. Rapid crosslinking likely results in an amorphous zirconium dioxide phase, which is beneficial for nitridation.[25,26] The powder X-ray diffractogram (PXRD) of the unpyrolyzed mixture with a molar ratio of urea to zirconium **U** of 15 (U15) without admixture of calcium dichloride is shown in Figure S2a in the supporting information. The mixture consists by sol-gel synthesis of mainly urea, zirconium dioxide, and remaining ammonium chloride. This is mirrored in the PXRD. The peak at 30.42° can be assigned to t-ZrO_2, but otherwise does not match the pattern of t-ZrO_2 well. The other marked peaks (22.20°, 24.58°, 29.28°, 35.46°, 37.06°) match urea more or less well in their position. Thus, the unpyrolyzed mixture likely consists of amorphous zirconium dioxide with well dispersed urea. The commercial nanoparticulate zirconium dioxide used for carbothermal nitridation is shown in Figure S2b. It matches m-ZrO_2 well and was used as supplied. Purposely crosslinking the sol by polycondensation after addition of urea and calcium chloride, followed by drying at 60 °C, results in a pourable, easy and safe to handle powder. The rapid crosslinking might also preserve the state of molecularly mixed components, which would be beneficial for the pyrolysis. The powder can be stored at room temperature and atmosphere without apparent detrimental effect on the pyrolysis result.

2.3. Effect of Pyrolysis Temperature

The following section shows the effect of the pyrolysis temperature on the occurring phases by X-ray diffraction (XRD). The pyrolysis temperature is a critical process parameter, because a high enough temperature is necessary, but not sufficient in itself. A sufficiently high urea content is also needed. A molar ratio of urea to metal U of 15 (U15) was established in prior experiments to synthesise ZrN at 900 °C.

Figure 1 shows powder X-ray diffractograms (XPRD) of samples with a molar ratio of 15 (U15), pyrolyzed at different temperatures of 800 °C, 900 °C, 1150 °C and 1400 °C with a dwelling time of 3 h, with exception of the highest temperature.

The PXRD pattern at 800 °C (Figure 1a) is complex, consisting of a diverse mixture of likely oxide and oxynitride. As expected, no ZrN-phase is obtained at a pyrolysis temperature of 800 °C.[9] It has to be noted, that this pyrolysis was done using a glassy carbon boat with a lid in contrast to the 900 °C and 1150 °C sample shown in Figure 1. The major peak at 34.01° can be attributed to ZrN but should be accompanied by a peak of similar intensity at 39.4°, which is absent (see 900 °C, Figure 1b). Still, a successful synthesis of ZrN at 800 °C using UGM is reported in literature, using a lower urea content and higher heating rate.[27] Nevertheless, synthesising ZrN at 800 °C following these reported parameters did not succeed in our work, in contrast to the reference.

A major cubic ZrN-phase (33.94°, 39.38°, 56.92°, 67.94°, 71.4°, 84.75°) emerges at 900 °C (Figure 1b) along with minor phases. The oxynitride phases (γ, β, β′) are difficult to distinguish by PXRD (Figure S1b). There is also pattern overlap with monoclinic (m) and tetragonal (t) zirconium dioxide (Figure S1c). The clearly visible peak at 30.41° can be assigned to either oxynitride or oxide, allowing for a small shift. However, the small peaks visible upon close inspection of the background at 21.47° and 45.62° match the γ-phase without any pattern overlap with the other regarded phases shown in Figure S1. The peak at 26.5° does not fit any of the mentioned dioxide or oxynitride patterns well. The peak at 28.27° can tentatively be assigned to m-ZrO_2 allowing for a small shift. The remaining peaks (28.27°, 35.18°, 50.71°, 60.33°) again can be assigned to either one of the oxynitride or dioxide phases. The amorphous region spanning from 20° to 35° can in part be caused by the used glass substrate, which does span a similar region.[28] However, an amorphous region is visible in the same range for the crystallisation of amorphous zirconium hydroxide $Zr(OH)_4$, which points to similar processes.[29] Regardless of the minor phases, synthesis of ZrN was successful at 900 °C. A minimum temperature of 900 °C concurs with the quasi-binary ZrO_2-Zr_3N_4

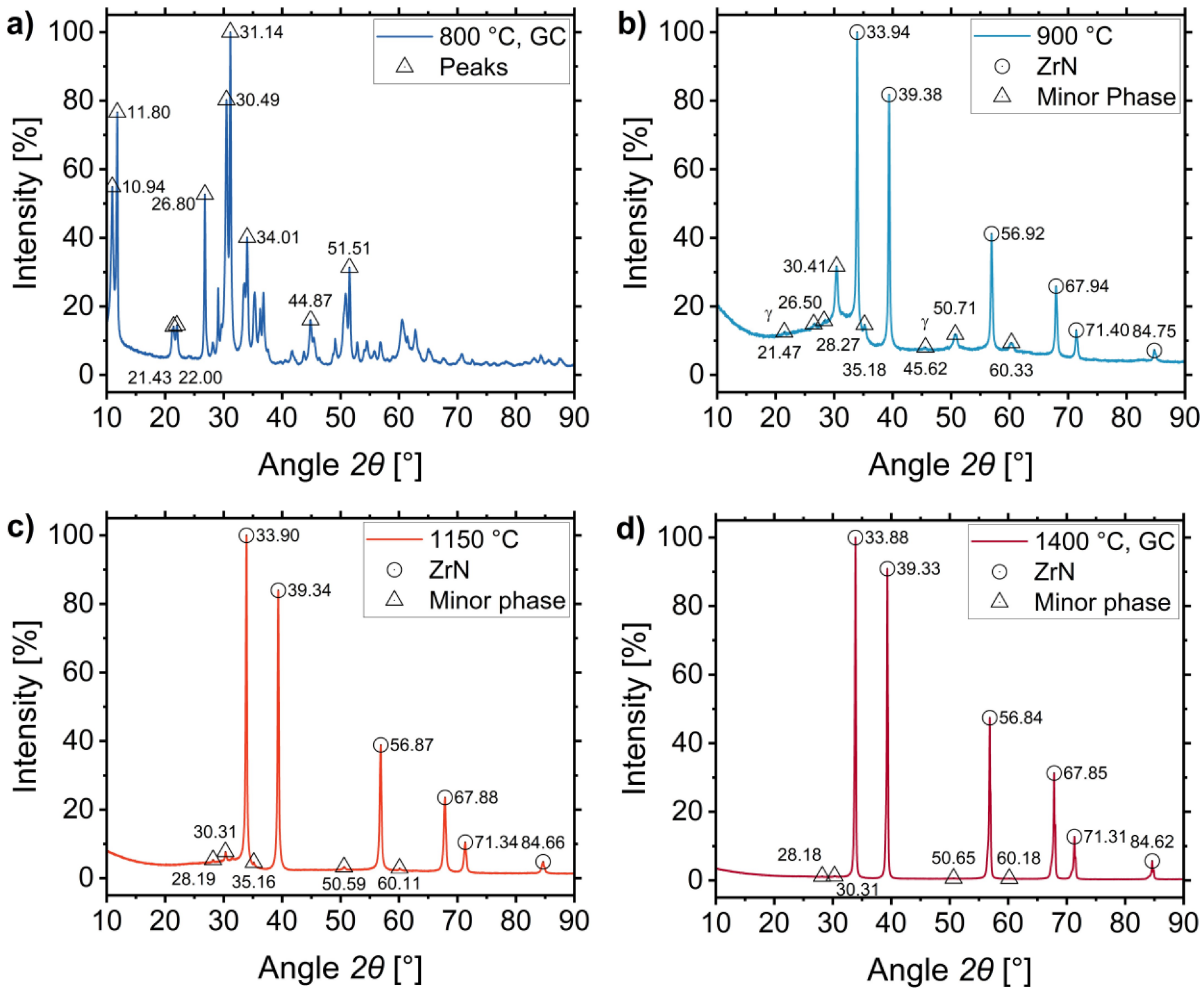

Figure 1. PXRDs of sample coatings on glass pyrolyzed at 800 °C (a) (III), 900 °C (b) (VI), 1150 °C (c) (X) and 1400 °C (d) (XII). A glazed alumina combustion boat (B) with an unglazed alumina lid (L) open at the ends was used at 900 °C and 1150 °C. A different kind of crucible, a glassy carbon (GC) boat, was used at 800 °C and 1400 °C.

phase diagram given by M. Lerch, in which nitrogen-rich zirconium oxynitride phases irreversibly decompose to ZrN, nitrogen and oxide or oxynitride, depending on the decomposing oxynitride phase and temperature.[9] Nitrogen diffusion seems to be the rate controlling factor for the conversion. The phase diagram by M. Lerch was constructed from sintering defined mixtures of ZrO_2 and Zr_3N_4, resulting in the described phase diagram.[9] Although the pyrolysis mixture does not consist of such a mix, the conversion to the nitride seems to occur similarly via an oxynitride phase starting from the dioxide. These conversion processes could also be the cause for some peak shifts as a result of non-stochiometric phases or defects.

Increasing the pyrolysis temperature to 1150 °C (Figure 1c), results in smaller peaks of the minor phases, indicating lower residual amounts of likely zirconium dioxide. The peak at 28.19° again fits m-ZrO_2. The remaining small peaks (30.31°, 35.16°, 50.59°, 60.11°) can be assigned to either oxynitride phase. However, the characteristic γ-peaks at 21.47° and 45.62° have vanished. Also, there is a small shift of all ZrN peaks to smaller 2θ angles by 0.04° to 0.09°, pointing to carbon incorporation. Regardless, an increased pyrolysis temperature of 1150 °C is beneficial to reduce undesired minor phases.

Increasing the temperature further to 1400 °C (Figure 1d) results in minor peaks barely above the background alongside the ZrN pattern, the hitherto cleanest ZrN pattern. The diminishingly small peaks at 28.18°, 30.31°, 50.65° and 60.18° are the same as before. This does not exclude some remaining oxygen in the ZrN crystal lattice. Furthermore, there is no visible amorphous region anymore, which can also be due to the scaling to the highest intensity peak. Regardless, the amount of minor phase is much reduced. The increased pyrolysis temperature from 900 °C to 1400 °C is accompanied by a small shift of the ZrN peaks to lower angles of 0.06° 2θ (33.94° to 33.88°), which is greater than estimated deviations (SI S12). This shift to lower angles is indicative of incorporation of carbon into the ZrN lattice, increasing the lattice parameter. It is well known that zirconium nitride is easily contaminated by oxygen and carbon.[16,17,30] This solid solution is often abbreviated as Zr(N, O, C). While the effect of oxygen on the lattice parameter is negligible depending on magnitude, carbon incorporation results in a noticeable shift.[17] This shift caused by the solid

solution of ZrN and ZrC can be quantitatively described by Vegard's Law. However, this calculation is very sensitive to the determined lattice parameter of the solid solution and chosen reference lattice parameters. Vegard's Law was used exemplarily in the comparison of synthesis methods (Table 2). The urea decomposition during the pyrolysis results in residual carbon in the pyrolysis mixture. The more urea, the more residual carbon may remain after pyrolysis, which may have been incorporated into the lattice to a greater extend as well.

Synthesis of zirconium nitride by UGM is possible above a pyrolysis temperature of 800 °C. The minor oxynitride and oxide phase, occurring alongside the nitride at 900 °C, are diminished with increasing pyrolysis temperature. There is no noticeable minor phase at 1400 °C anymore. However, the increased pyrolysis temperature is accompanied by a small shift of the peaks to lower angles, indicating undesired carbon incorporation into the crystal lattice i.e. a reduced purity of the nitride.

2.4. Effect of 'Calcium' Admixture

The following section shows the effect of adding calcium ions to the sol-gel on the synthesis of zirconium nitride as described by Gao et al. for tantalum nitride.[15] To this end, calcium dichloride was added in a molar ratio to the zirconium tetrachloride. This admixture of calcium dichloride is simply referred to as 'calcium admixture' in the following text and is denoted by '*Ca*' followed by the ratio as a number. The added calcium ions slow the urea decomposition and in turn the release of reactive nitrogen species. The effect thereof on the conversion of the likely amorphous oxide precursor to the desired nitride phase was investigated by varying the calcium admixture. The effect of added calcium ions on the thermal decomposition of pure urea was investigated by thermogravimetric analysis (TGA), showing a slowed down decomposition (SI S4). Shown below are PXRDs of samples with a calcium admixture of *Ca0.25*, *Ca0.5*, *Ca1.0*, and *Ca2.0*.

A calcium admixture as low as *Ca0.25* (Figure 2a) results in the visible occurrence of oxynitride (and oxide) as minor phases alongside a major ZrN-phase (33.98°, 39.44°, 56.99°, 68.04°, 71.51°, 84.66°). The different oxynitrides are difficult to distinguish by PXRD due to their similar lattice parameters.[31] There is also pattern overlap of the oxynitrides with t-ZrO_2 and m-ZrO_2 (Figure S1c). The noticeable peak at 10.97°, indicating a large lattice distance, is likely caused by a layered structure such as layered double hydroxides.[32,33] Large thin plate-like structures with small homogeneously embedded nanoparticles were observed in TEM images for samples with calcium admixture (Figure 4), pointing at this explanation. However, the formation of some compound of zirconium with calcium is also a possible explanation. Some form of nucleation seems to originate within these structures (Figure 4b). The peak at 21.44° is matched only by the γ-phase, Zr_2ON_2. Although the angles are slightly too large, the peaks at 30.53° and 35.41° can be assigned best to the γ-phase as well. The amorphous region occurring for this composition without calcium is absent.

Table 2. Stoichiometry by Vegard's law and residual carbon content by oxidation for selected samples synthesised by urea-glass method (UGM) and high temperature carbothermal nitridation (CN).

Sample	Vegard's Law	Residual carbon w_C
UGM: *Ca0.0*, 1400 °C, 2 h (XII)	$ZrN_{0.93\pm0.05}C_{0.07\pm0.05}$	13.8 ± 1.2 %
UGM: *Ca0.5*, 1150 °C, 3 h (XVII)	$ZrN_{0.95\pm0.05}C_{0.05\pm0.05}$	6.2 ± 1.4 %
CN: C4, 1400 °C, 3 h (XXIII)	$ZrN_{0.63\pm0.17}C_{0.37\pm0.17}$	16.3 ± 3.7 %
CN: C4, 1400 °C, 4.5 h (XXV)	$ZrN_{0.90\pm0.05}C_{0.10\pm0.05}$	20.3 ± 1.1 %
CN: C2, 1400 °C, 4.5 h (XXIV)	$ZrN_{0.91\pm0.05}C_{0.09\pm0.05}$	−0.2 ± 2.1 %

An increased calcium admixture of *Ca0.5* results in the highest relative intensity of the ZrN phase for all tested calcium contents. Further increasing the calcium admixture resulted in less ZrN by intensity in relation to the other phases. The nitride becomes a minor phase at *Ca2.0*, where the γ-phase becomes dominant. An increasing peak intensity at 10.97° coincides with reduced intensity of ZrN. The same trend occurs for the γ-phase peak at 30.53°. These similar trends diverge at *Ca2.0*, where the γ-phase is dominant, but the peak at 10.97° is at a slightly lower intensity than in *Ca0.25*. This trend and divergence can be explained by a decomposition of γ-phase to nitride.[9] The conversion seems to be accompanied by the layered structure causing the peak at 10.97°. The less γ-phase decomposes, the less nitride forms, the less layered structure occurs, in which possibly some form of nucleation happens. It is uncertain, whether this structure forms from decomposition the γ-phase or itself forms the nitride. However, the peak at 10.97° is not visible at a lower urea content of U5 (Figure S9–S11), neither with calcium, when no nitride forms, nor without calcium, when some nitride forms. The γ-phase is dominant in both cases. Noteworthy as well is a shift of the ZrN peaks to slightly higher angles with increasing calcium content, which could be caused by higher nitride purity i.e. closer to a perfect stoichiometry (Figure S6). Although the effect of oxygen on the lattice parameter of ZrN is low, it results in a shift to lower Bragg angles.[17] The slight shift to higher angles observed with calcium admixture might indicate less oxygen in the ZrN lattice. Lerch and Wrba give a slightly lower lattice parameter for ZrN, generated from decomposition of Zr_3N_4, of 0.45569(4) nm than Constant et al. with 0.4571 nm (−0.3 %), which yields Bragg angles at the observed higher values with calcium admixture (Figure S1a).[16,17] Ammonolysis of $ZrCl_4$ in flowing ammonia at 850–950 °C results in Zr_3N_4,[34] but only if there is no oxygen present, otherwise oxynitrides form.[31] In consequence, ZrN formed from decomposition of Zr_3N_4 should contain one of the least amounts of oxygen in the crystal lattice. Lattice parameters derived from this ZrN should be close to the true value.

Based on this interpretation, the conversion of amorphous ZrO_2 to ZrN happens by successive conversion of the oxide to oxynitrides with increasing nitrogen content. These oxynitrides in turn decompose into nitride, oxynitride and nitrogen (see scheme below).

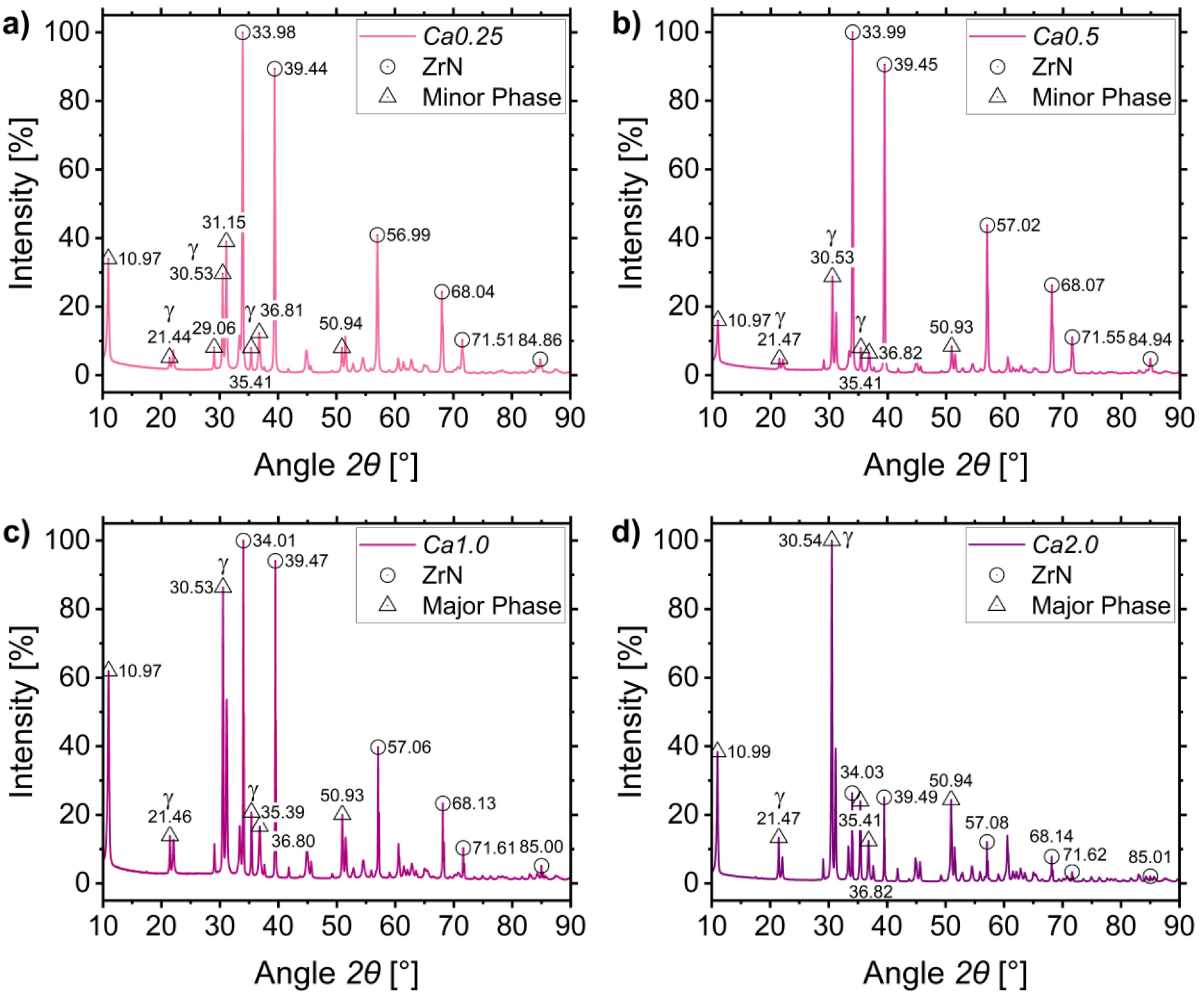

Figure 2. PXRDs of sample coatings on glass pyrolyzed at 900 °C for 3 hours with calcium admixtures of *Ca0.25* (a) (XIII), *Ca0.5* (b) (XIV), *Ca1.0* (c) (XIX) and *Ca2.0* (d) (XXI) respectively.

$$ZrO_2 \rightarrow Zr_7O_{11}N_2\ (\beta') \rightarrow Zr_7O_8N_4\ (\beta) \rightarrow Zr_2ON_2\ (\gamma) \rightarrow ZrN + \beta + N_2$$

Following the quasi-binary phase diagram given by Lerch, γ decomposes to nitride, β and nitrogen above approximately 840 °C and below 1000 °C.[9] Assuming γ-phase decomposes stoichiometrically (Equation (1)) and disregarding other components such as residual carbon, the achievable ZrN mass fraction via this conversion is only 54 % (Equation (2)).

$$16\ Zr_2ON_2 \rightarrow 2\ Zr_7O_8N_4 + 18\ ZrN + 3\ N_2 \quad (1)$$

$$\frac{18\ M_{ZrN}}{18\ M_{ZrN} + 2\ M_{Zr_7O_8N_4}} = \frac{18 \cdot 105.2307}{18 \cdot 105.2307 + 2 \cdot 822.5868} \approx 54\ \% \quad (2)$$

Though, if the gradual nitridation of ZrO_2 takes place continuously by a retained local atmosphere, and not solely via decomposition of an early evolved glassy intermediate, then the oxynitride by-product is nitrided again and in turn decomposes to form nitride and oxynitride (see scheme below).

$$\beta \rightarrow \gamma \rightarrow ZrN + \beta + N_2$$

The amount of ZrN was determined exemplarily for one sample using XRD by standard addition of commercial ZrO_2, giving a mass fraction of about 90 %. This much higher mass fraction than the theoretical value supports the assumption of a continuous cycle as long as there are reactive nitrogen species. An increased dwelling time should result in more nitride under these circumstances, but only if this reservoir of nitriding atmosphere is retained, not already depleted and the phases are not yet in equilibrium. However, an increased dwelling time of 4.5 h (50 % increase) had no significant effect at 900 °C with or without added calcium dichloride, with the exception of an approximately halved peak intensity at 30.53° for *Ca0.5* (SI S8). Calcium admixture slows the urea decomposition and release of reactive nitrogen species based on its effect on the phase composition, which depends on the amount of calcium ions added. The slowed release results in an oxynitride instead of oxide minor phase occurring alongside the major ZrN phase. The cause is either a better utilisation of the available, more slowly released reactive nitrogen species, converting more

oxide, or it is as yet undecomposed oxynitride. A large admixture inhibits the conversion of the oxide to the nitride.

2.5. High–Temperature Synthesis – Carbothermal Nitridation

A carbothermal nitridation (CN) synthesis of zirconium nitride (Equation (3)) becomes possible at a temperature of 1400 °C, at which zirconium dioxide can be nitrided directly by a nitrogen atmosphere.[16] A classical CN of ZrN was tested in comparison to the UGM using a high-temperature oven and a mixture of commercial ZrO_2 and carbon black. The added carbon acts as oxygen getter reducing the ZrO_2, for which the theoretical stoichiometric ratio is 2 (Equation (3)).

$$2\ ZrO_2(s) + N_2(g) + 4\ C(s) \rightarrow 2\ ZrN(s) + 4\ CO(g) \quad (3)$$

A molar ratio of C to ZrO_2 of 4 (C4) resulted in a single Zr(N,C) phase with a noticeable shift of $\leq 0.38°$ to lower angles at a dwelling time of 3 h, which is indicative of a large ZrC fraction in the solid solution of ZrN and ZrC (Figure S16). This was alleviated by an increased dwelling time of 4.5 h (Figure S16). The large amount of remaining added carbon after pyrolysis (Table 2) was remedied by reducing the molar ratio to the theoretical stochiometric ratio of C2. Although C2 prevents residual carbon, it also results in a small minor oxide phase. This optimised CN product as well as UGM 1400 °C and UGM 1150 °C *Ca0.5* are shown in Figure 3 for comparison. All three PXRDs shown a major ZrN phase, with a varying shift to lower angles, which is caused by carbon in the ZrN lattice. The stoichiometry of this solid solution of ZrN and ZrC was evaluated by Vegard's law. However, the lattice parameters of the pure phases, ZrN and ZrC, are required. These data are optimally generated on the same setup with the identical systematic measurement error. In absence of that, suitable reference data can be used. The lattice parameters of ZrN and ZrC as well as mixtures thereof given by Constant et al. were linearly fitted (SI S13).[17] Lattice parameters of $a_{ZrN} = 0.4571$ nm and $a_{ZrC} = 0.4695$ nm were used for calculations. All peaks shown were included in the calculation, weighted by their peak intensity and averaged. A linear error propagation was used to calculate a standard deviation. The stoichiometries calculated this way are $ZrN_{0.91\pm0.05}C_{0.09\pm0.05}$ (CN), $ZrN_{0.93\pm0.05}C_{0.07\pm0.05}$ (UGM 1400 °C) and *Ca0.5* $ZrN_{0.95\pm0.05}C_{0.05\pm0.05}$ (UGM 1150 °C) (Table 2). Although all three calculated stoichiometries are similarly pure in regard to the nitride, they show that a higher synthesis temperature results in a larger amount of undesired carbon incorporated in the crystal lattice. Higher temperatures enhance carbon incorporation, the carbide is more stable than the nitride at high temperatures.[35] Yet a minimum temperature of 1400 °C is needed for direct nitridation of ZrO_2 in nitrogen.[16] Likely cause of the larger ZrC fraction of the CN sample lies within the reaction mechanism. CN works by conversion of the ZrO_2 to ZrC, which in turn is converted into ZrN.[36,37] A further increased dwelling time might remove both the ZrC fraction and minor oxide phase. In contrast, the nitrides synthesised by UGM at 1400 °C and 1150 °C with *Ca0.5* do not contain significant carbon in the crystal lattice as determined by Vegard's Law, which is the desired outcome, a pure ZrN. Both UGM samples contain small amounts of oxynitride, less so at 1400 °C than at 1150 °C. All three samples were oxidized in pure oxygen using a TGA to

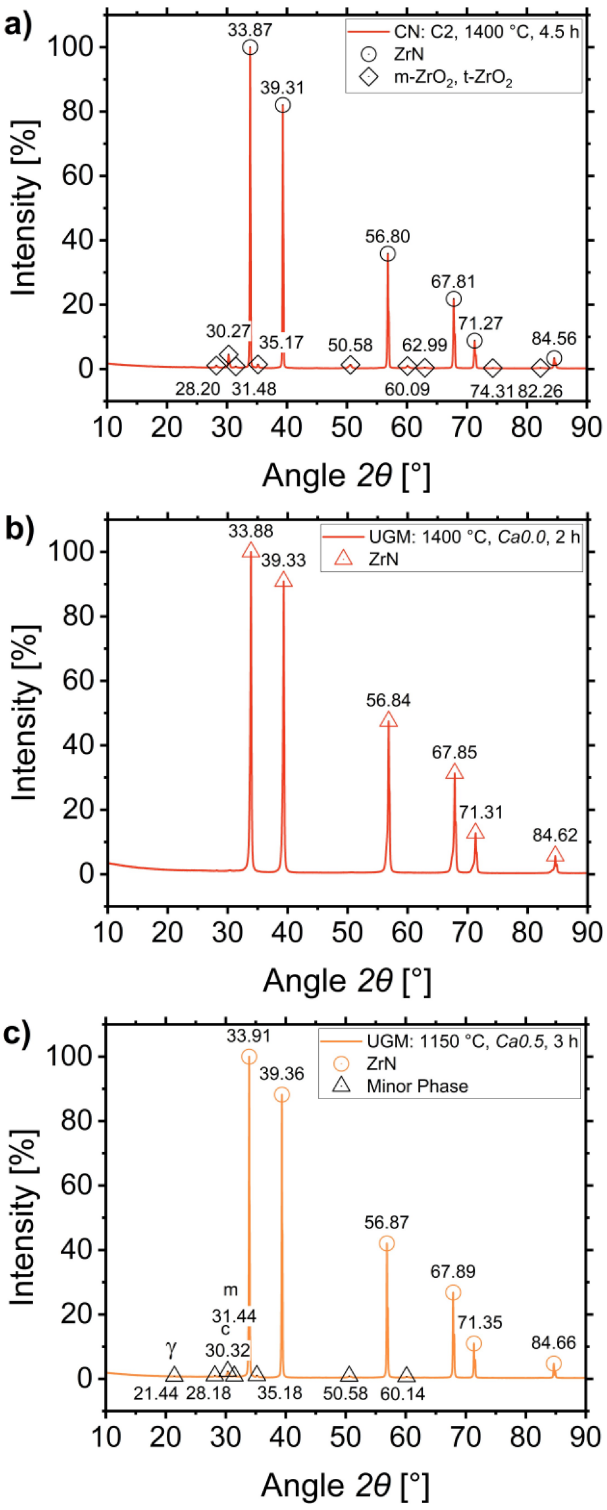

Figure 3. PXRDs of sample coatings on glass pyrolyzed at 1400 °C via CN (a) (XXIV), UGM (b) (XII) and at 1150 °C with *Ca0.5* (c) (XVII).

derive the amount of residual carbon remaining after pyrolysis and washing (SI S14). The carbon mass fraction in the unoxidized sample was derived from the change in mass assuming complete oxidation and conservation of the amount of zirconium. The stoichiometry derived by Vegard's Law was used to calculate the molar mass. Other impurities such as oxynitrides were discounted. The carbon mass fraction calculated this way were in order $-0.2 \pm 2.1\%$, $13.8 \pm 1.2\%$ and $6.2 \pm 1.4\%$ (Table 2). The CN sample does not contain residual carbon, which is desired. The UGM 1150 °C *Ca0.5* sample contains less residual carbon than UGM 1400 °C, as expected. One effect of calcium admixture is reduction of residual carbon.[15]

Both synthesis methods allow to synthesise relatively pure nanocrystalline ZrN. UGM achieves a higher ZrN purity in regard to ZrC, but at a much lower synthesis yield with some remaining residual carbon and general more complex synthesis mixture. CN results in slightly lower nitride purity, but at higher synthesis yield with no residual carbon, albeit with a minor oxide phase at the current synthesis parameters, and always requires a higher pyrolysis temperature.

2.6. Influence of the Synthesis on observed Particle Morphologies

Particle size and morphology were qualitatively assessed by TEM, a representative selection of samples and particles is shown in Figure 4. The samples generally showed aggregates and agglomerates of small and large particles as shown in Figures 4a, c, d and f. Large particles were in the range of 50–100 nm, while small particles were in the range of 10–20 nm. Particles, large and small, separate or in aggregates, often locally showed a core-shell structure visible in the contrast (Figure 4d). This shell likely consists of zirconium dioxide or residual carbon, albeit an oxide shell is more likely, either by surface oxidation or in consequence of the reaction mechanism. Admixture of calcium (Figures 4b, f) resulted in the additional occurrence of large plate-like particles as shown in Figure 4b. It is suspected that these structures are responsible for the PXRD peak at 10.9°. Small nanoparticles in the range of 2–5 nm were evenly embedded in some of these plate-like structures (Figure 4b). Further investigation of these particles via HR-TEM and EDS was not possible, because they disintegrated upon irradiation at higher acceleration voltages typical for HR-TEM (200 kV). Calcium admixture also resulted in some much larger cubic particles in the range of 500–1000 nm (Figure 5), indicating higher crystallinity. This observation matches the higher intensity of PXRD patterns and $K\alpha_1$-$K\alpha_2$-splitting seen for samples with calcium admixture (Figure S15).

HR-TEM brightfield and selected area electron diffraction (SAED) images were used to determine d-spacings (SI S16). Reference d-spacings were taken from the used ICDD PDF cards. While both brightfield images and SAED yield d-spacings which can be assigned to ZrN and ZrO_2 for samples with and without calcium admixture, SAED also yields d-spacings that can be in part tentatively assigned to oxynitride phases, affirming the generally observed phases by PXRD. The elemental composition was analysed by EDS for the same two samples. Figure 5 exemplarily shows the EDS measurement of the sample with calcium admixture Ca0.5 pyrolyzed at 900 °C. All EDS measurements showed a largely homogeneous elemental distribution in regard to the examined elements (Zr, N, C, O). Detected Zr is spatially localized to particles, most notably for the approximately 500 nm particle in the top of the image. High N concentrations coincide well with Zr and thus the particles, indicating ZrN particles. However, O shows a similar local distribution. This points to either a surface oxidation, oxide or oxynitride shell. Both N and O show a higher concentration towards the particles fringe. This also points to a surface oxidation or assumed conversion of an oxynitride to a nitride. The diffusion rate of oxygen is higher than that of nitrogen, resulting in a N gradient towards the centre, which was observed by Zhao et al. for ZrN synthesized by CN.[9,37] Particle geometry, thickness and edge orientation can cause a higher local concentration as well e.g. more detected N and O at the edge of a particle. Having said this, N and more so O also coincide locally with C outside of particles. The Formvar grid coating as well as the residual carbon can be the cause, contributing to the background. Residual carbon probably precipitates around particles during the synthesis and accumulates, as a carbon shell forms in case of chromium nitride nanoparticle formation by UGM.[14] Calcium and chloride were also detected with some localisation at the particles (Figures S21 and S22). Chloride ions likely remain from the used zirconium tetrachloride precursor, added calcium chloride or acid-washing with hydrochloric acid. Because both elements are more or less evenly dispersed throughout the sample, it is assumed both are residues. The elements quantified by EDS are given in the Table S7. The surface composition determined by XPS has been included for sake of comparison. The XPS results will be discussed in detail in a separate section. Both samples show a higher carbon content by EDS than XPS. Oxygen shows the opposite trend, a much higher oxygen content by XPS than EDS, which is attributed to the expected surface oxidation. Whether this suspected oxide shell forms during synthesis, after pyrolysis or during handling in normal atmosphere is uncertain. XPS in contrast to EDS is a surface sensitive spectroscopy with a penetration depth of a few nanometres. The ratio of oxygen content by XPS to EDS is of similar magnitude for both samples, with and without calcium admixture. Calculating the composition from EDS as a rough estimate results in a stoichiometry of $ZrO_{0.34}N_{1.05}$ with and $ZrO_{1.02}N_{1.34}$ without calcium admixture discounting carbon, indicating Zr(N, O) phases. The thus calculated stoichiometry of the sample with calcium admixture is close to the γ-phase, Zr_2ON_2, which occurs with calcium admixture among other oxynitride phases as determined by PXRD. Although the effect of dissolved oxygen on the lattice parameter is small, the stoichiometry of the sample without calcium determined from EDS, $ZrO_{1.02}N_{1.34}$, does not fit well with the determined PXRD pattern, which is matched to ZrN as main phase.[17] Oxygen in the lattice has been linked to vacancies in the metal sublattice.[30] Comparing the X-ray density ρ_x calculated from the unit cell, assuming complete occupancy of the

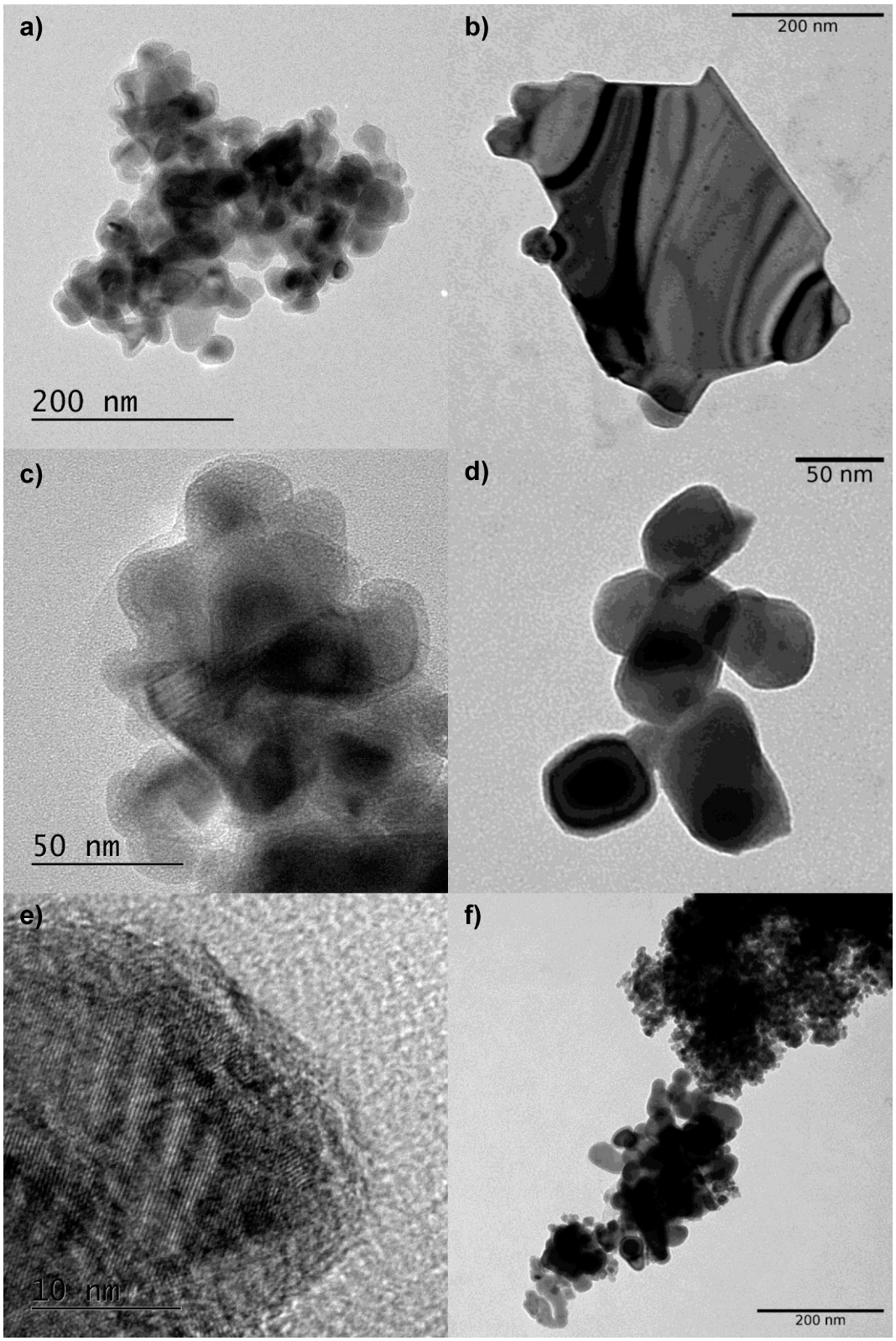

Figure 4. TEM and HR-TEM images representative of the particle size and morphology encountered for different synthesis compositions and pyrolysis conditions: (a, c, e) *Ca0.0*, 900 °C (VI), (b) *Ca0.5*, 900 °C (XIV), (d) *Ca0.0*, 1150 °C (X), (f) *Ca0.5*, 1150 °C (XVII).

metal sites, to the actual powder skeletal density ρ_p, disregarding closed pores, allows to calculate the vacancy density, which is likely caused by dissolved oxygen. Determining the powder skeletal density by gas pycnometry is in principle a simple task. However, this is hampered by insufficient sample volume for accurate measurements and, beyond that, fails due to the

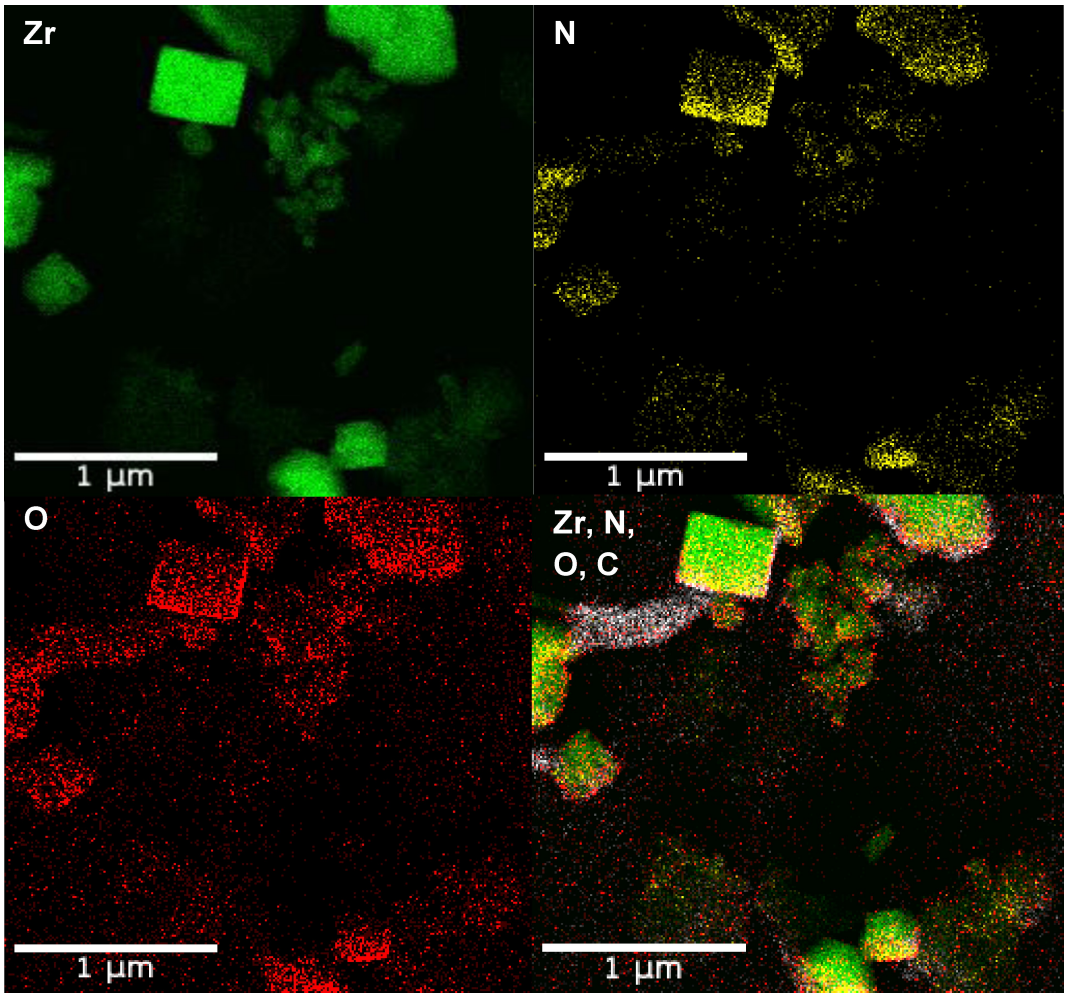

Figure 5. EDS measurement of the TEM sample *Ca0.5*, 900 °C (XIV) showing the elemental composition for Zr, N, O and combined with C. The colour balance has been adjusted for the light elements N, O, C.

residual carbon, which has a much lower, unknown density. The measured density would have to be corrected for this unknown density. A powder skeletal density of $5.334 \pm 0.04\ g\,cm^{-3}$ was determined for the sample pyrolyzed at 1150 °C with *Ca0.5*. Assuming a density range of less than $1\ g\,cm^{-3}$ for amorphous carbon to $2.3\ g\,cm^{-3}$ for graphite results in a nitrogen vacancy concentration of 0.03 to 0.22. The composition determined by Vegard's law of $ZrN_{0.95\pm0.05}C_{0.05\pm0.05}$ should correspond to a nitrogen vacancy concentration of approximately 0.1 in published data, which roughly fits the estimated range.[30] Taken together, this indicates the synthesised material is ZrN as determined by XRD, but the surface is oxidized and there is some dissolved oxygen in the lattice.

2.7. Surface Composition of Zirconium (oxy)nitride Materials

XPS measurements were performed to analyse the surface composition of the prepared ZrN-based materials in respect to the varied parameters and synthesis routes. TMNs are prone to surface oxidation. Thus, a surface oxide layer is expected on successfully synthesized ZrN particles. Even though sputter cleaning of the pristine samples can remove the surface oxide layer, it was not performed, because of preferential sputtering of certain elements. This would result in artificial variation of the atomic concentrations or cause cascade mixing, where one element is smeared along deeper levels than in the pristine sample. Tose effects also obscure an exact assignment of core level binding energy (BE) values.[38,39]

First, samples synthesised by UGM pyrolyzed at 900 °C are discussed according to the calcium admixture. Survey spectra are presented in the supporting information (Figure S14), showing the expected elements Zr, N, O and C alongside contaminations from the synthesis and sample processing, mainly Ca and Cl. The peak-deconvoluted high-resolution Zr 3d, N 1s and O 1s spectra are shown in separate columns in Figure 6. Each row pertains to one sample pyrolyzed at 900 °C with varying calcium admixture (*Ca0.0*, *Ca0.5*, *Ca1.0*, *Ca2.0*), starting at the top with no calcium admixture (*Ca0.0*). The Zr 3d spectra consist of spin-orbit doublet peaks (Zr $3d_{5/2}$ and Zr $3d_{3/2}$), which were fitted with three components corresponding to zirconium nitride (z1), oxynitride (z2) and oxide (z3) phases.[39,40] The high-resolution N 1s spectra were fitted with four

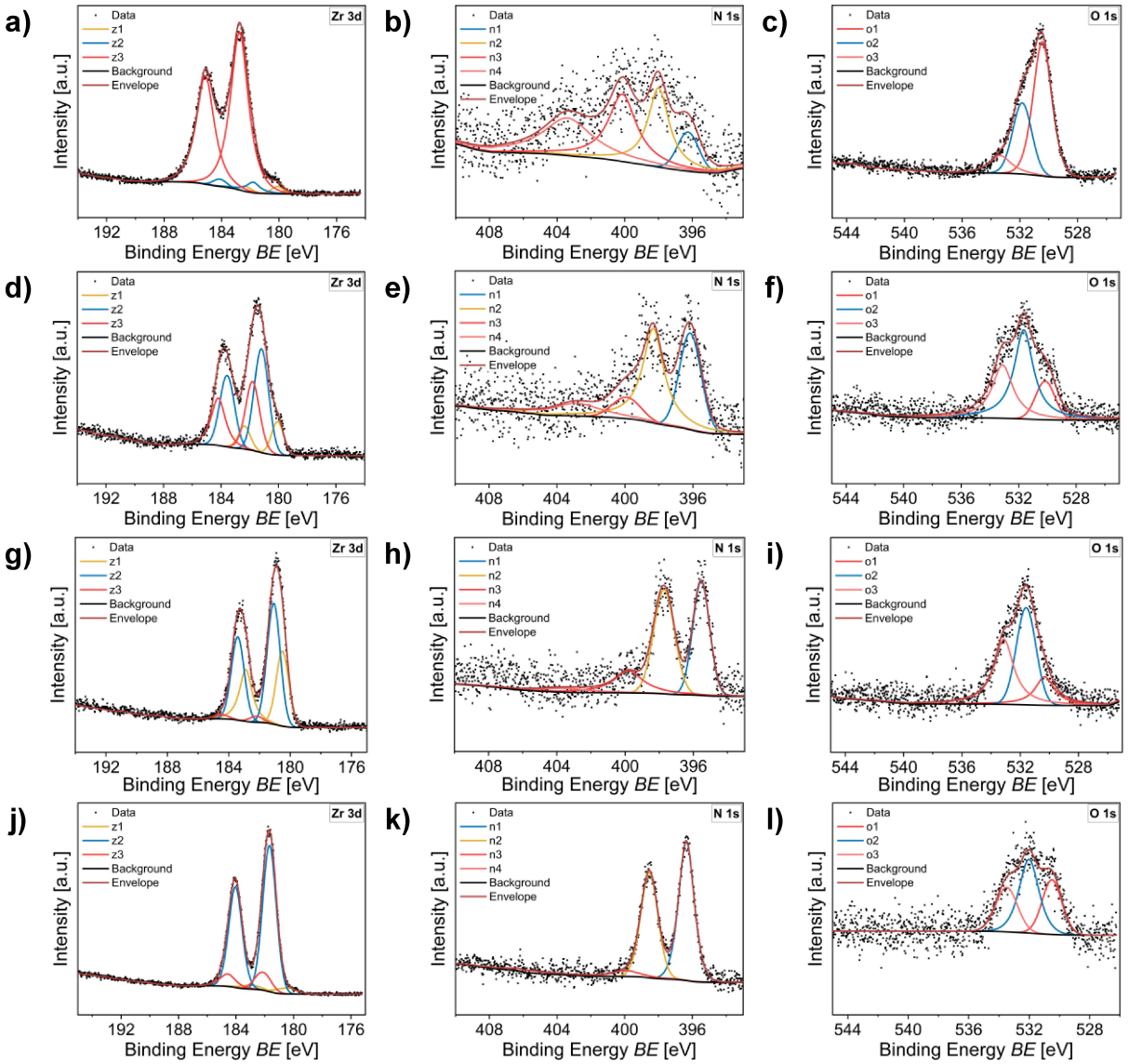

Figure 6. XP spectra of samples with varying calcium admixture (*Ca0.0*, *Ca0.5*, *Ca1.0*, *Ca2.0*) pyrolyzed at 900 °C for 3 hours. The peak-deconvoluted high-resolution Zr 3d, N 1s and O 1s spectra are shown by column: (a–c) *Ca0.0*, (d–f) *Ca0.5*, (g–i) *Ca1.0*, (j–l) *Ca2.0*

components corresponding to oxynitride (n1), nitride (n2) and adsorbed nitrogen species (n3), as well as adsorbed molecular N_2 (n4).[39,41,42] It has to be noted that a low nitrogen concentration was measured by XPS due to supposed surface oxidation of the major nitride phase, resulting in a low signal to noise ratio of the N 1s spectrum. The N 1s spectra were nonetheless fitted to illustrate changing contributions of the components among the synthesized materials. The O 1s spectra were fitted with three components corresponding to oxide (o1), adsorbed oxygen/hydroxide species (o2) and adsorbed water (o3).[39,42] Correction of the recorded binding energies was accomplished by using the shift of the aliphatic carbon signal (component c1 in C 1s spectra, Figure S15) to a BE of 248.8 eV.[43] Further components (c2–c5) belong to oxidized carbon species from adventitious carbon, if not otherwise discussed below.

The calcium-free sample (Figure 6, a–c) is exhaustively oxidized at the surface as apparent from the zirconium dioxide peak, component z3, at a (BE of 182.8 eV (Figure 6a). This correlates with the low signal intensity of the N 1s spectrum (Figure 6b) and a high intensity of the oxide peak in the O 1s spectrum, component o1, at 530.4 eV corresponding to zirconium oxide (Figure 6c).[39] Slightly visible (oxy)nitride signals could originate from an underlying major nitride phase as determined by XRD (Figure 1b). Calcium admixture resulted in a gradual decrease of the nitride phase and increasing oxynitride phases as revealed by XRD. This trend is supported by XPS measurements. The samples with a calcium admixture of *Ca0.5* and *Ca1.0* (Figure 6d–i) markedly show a mixture of nitride, component z1 (180.1 eV and 180.5 eV), and oxynitride, component z2 (181.2 eV and 181.1 eV), in their respective Zr 3d spectrum (Figure 6d and g). This agrees with pronounced contributions of the oxynitride, component n1 (396.2 eV and

395.5 eV), and nitride, component n2 (398.3 eV and 397.7 eV), to the N 1s spectra (Figure 6e and h) as well as a decreased contribution of the oxide (o1, 530.2 eV and 530 eV) to the O 1s spectra (Figure 6f and i).[39,42] This trend of larger contribution of nitride and oxynitride components to the XP spectra, and at the same time diminished contribution of the oxide, with increasing calcium admixture is coherent with the observed changes in phase composition by PXRD i.e. increasing amount of oxynitride with increasing calcium admixture. In summary, the more oxynitride present in the sample, the less surface oxidation occurs in relation to the sample without calcium. An explanation for this observation is the decreasing oxidation enthalpy of oxynitrides with decreasing nitrogen content.[44] The oxynitrides do not oxidize as readily as the nitride.

In contrast to this trend, there are certain oxide components visible again in the Zr 3d (z3, 182.1 eV) and O 1s (o1, 540.5 eV) spectrum at the highest calcium admixture of *Ca2.0* (Figure 6j and l). The higher the calcium admixture, the slower the urea decomposition driving the conversion of the oxide to the nitride. In consequence, calcium admixture causes intermediate oxynitrides of varying nitrogen content to remain. If the conversion is slowed to an extent that the oxides are partially not transformed to oxynitride nor nitride during the synthesis in the first place, the oxidic precursor will partially remain and its oxide components are detected at the high calcium admixture. However, the N 1s spectrum (Figure 6k) still contains a pronounced nitride signal (n2, 398.5 eV), even though there is no corresponding signal in the Zr 3d spectrum (Figure 6l). It has to be noted that the correction of all XP spectra by the C 1s signal resulted in a large applied shift of the binding energies here, which might have caused the missing nitride signal in the Zr 3d signal. Regardless, this N 1s nitride signal can also be related to carbon nitride components of the amorphous carbon phase emerging in the UGM synthesis.[45] Pronounced C 1s and N 1s signals at 288.2 eV and 398.7 eV respectively have been reported for crystalline carbon nitrides e.g. C_3N_4. However, graphitic C_3N_4 is not readily apparent in our diffractograms. Furthermore, the C 1s spectrum (Figure S23d) also contains a pronounced signal at 287.6 eV (c3) that can originate from amorphous carbon nitride species in this sample. The larger ratio of n2 to corresponding z1 component at *Ca2.0* in relation to *Ca0.5* and *Ca1.0* points to amorphous carbon as cause as well.

The effect of the pyrolysis temperature on the surface composition in the UGM and CN synthesis route was evaluated by XPS next (Figure 7). An increased pyrolysis temperature of 1150 °C and 1400 °C facilitated the nitride formation independently of calcium admixture (Figure S15) and synthesis route (Figure 1 and Figure 3). A pyrolysis temperature of 1150 °C without calcium admixture resulted in a similar indication of surface oxidation (Figure S25) as discussed for the analogue 900 °C sample. A small calcium admixture of *Ca0.5* at 1150 °C

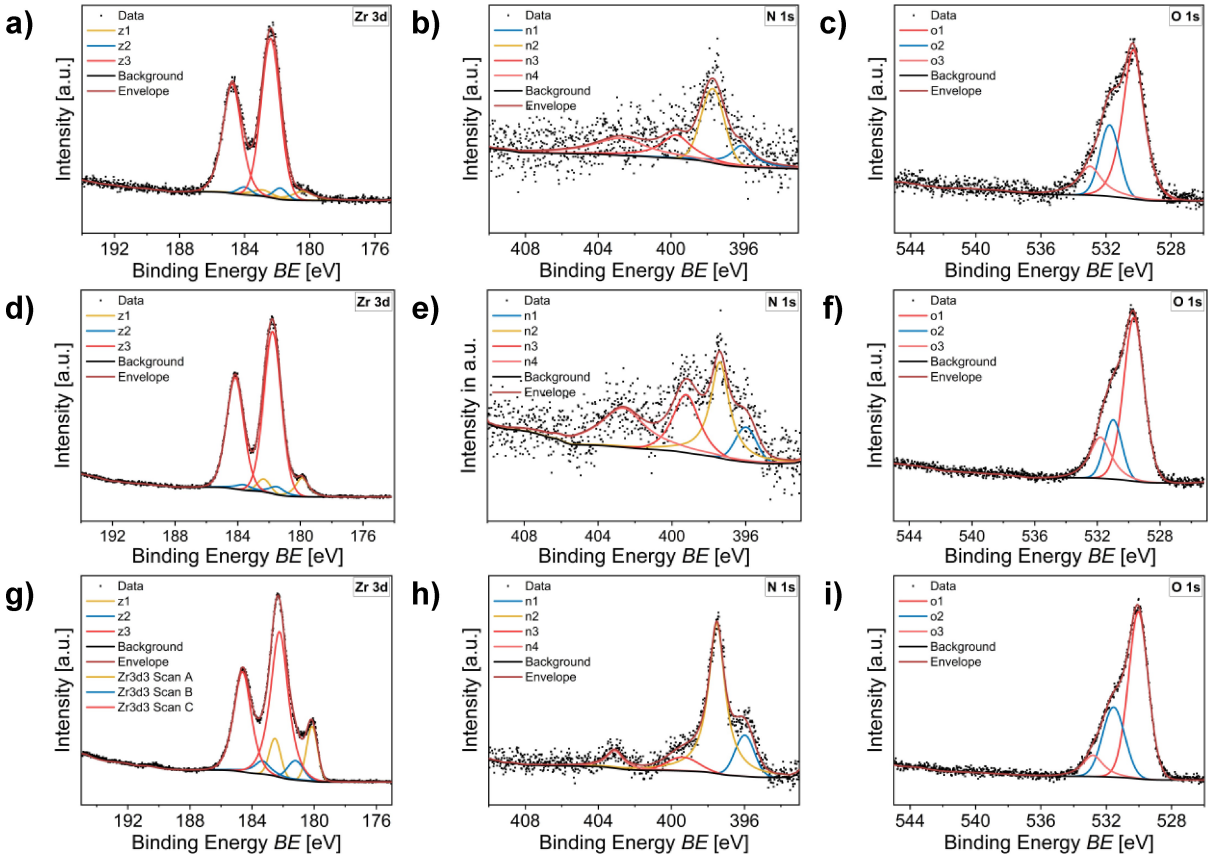

Figure 7. XP spectra of samples pyrolyzed at 1150 °C and 1400 °C via UGM and CN. The peak-deconvoluted high-resolution Zr 3d, N 1s and O 1s spectra are shown by column: (a–c) UGM, *Ca0.5*, 1150 °C, (d–f) *UGM*, 1400 °C, (g–i) CN, C2, 4.5 h

shows an increased intensity of the nitride component n2 (397.7 eV) (Figure 7b), whereas both the Zr 3d (z3, 182.4 eV) and the O 1s spectrum (o1, 530.3 eV) reveal the presence of a surface oxide layer. However, the in comparison higher intensity n2 component points to a thinner surface oxide layer, which yields more information from the underlying nitride phase. Additionally, the high-resolution C 1s spectra at a pyrolysis temperature of 1150 °C (Figures S25 and S26) show two additional components, c6 and c7, which correspond to graphite and its π to π* satellite, which might originate from graphitic carbon at the higher pyrolysis temperature of 1150 °C. A further increased pyrolysis temperature of 1400 °C results in very similar XP spectra (Figure 7d–f) but for the higher contributions of the nitride components (z1, 179.9 eV and n2, 397.4 eV), indicating a thinner oxide layer than at 1150 °C.

Finally, all three CN samples consist of a major ZrN phase by PXRD (Table 2), which shows an expected surface oxidation and thus similar XPS signals. However, the two samples with a higher carbon ratio of C4 show a larger contribution from residual graphitic carbon (c6, Figures S28b and S29b), both C4 samples contain significant carbon after the pyrolysis. The significant shift to lower angles apparent in the diffractogram at the lower dwelling time of 3 h (Figure S16) was attributed to a solid solution of nitride and carbide as evaluated by Vegard's Law (Table 2). The lack of distinct zirconium carbide signals in the XP spectra of this C4 sample substantiate the assumed solid solution of nitride and carbide i.e. partial substitution of nitrogen atoms by carbon instead of two distinct phases.[45] A higher dwelling time of 4.5 h rectified this undesired carbide fraction, and only a minor shift likely characteristic for the high synthesis temperature of 1400 °C remained. The last CN sample was synthesized with a halved carbon ratio of C2, because significant carbon remained before at C4 and C2 is the stoichiometric ratio. The reduced carbon ratio resulted in carbon free ZrN, albeit with a minor oxide phase by PXRD. The C2 sample also shows an oxidized surface (Figure 7) as apparent in the Zr 3d (z3, 182.2 eV) and O 1s (o1, 530.0 eV) spectrum respectively. Interestingly, the contribution of the nitride phase is clearly visible in the Zr 3d (z1, 180.1 eV) and N 1s (n2, 397.5 eV) spectrum and is also stronger compared to the other ZrN materials synthesized by UGM at 1150 °C and 1400 °C. Either the minor zirconium dioxide phase in the UGM samples contributes majorly to the XPS signals or a thinner surface oxide layer of the CN sample allows for a larger contribution of the underlying ZrN phase. In summary, the recorded XP spectra show the expected surface oxidation of the synthesized ZrN materials. The nitride phase (component n2) contributes to a different extent to the signals depending on the sample. This varying contribution, although all samples consist of ZrN as determined by XRD, is believed to be caused by a different surface oxide layer thickness. This hypothesis will have to be investigated further by HR-TEM measurements of suitable specimens. A reduced surface oxide formation was found for samples synthesized by Ca-assisted UGM, which has been related to the shift to less easily oxidized oxynitride materials by calcium admixture.

2.8. Electrochemical Characterisation – Nitrogen Reduction Reaction Activity

TMNs are potentially promising NRR catalysts because it is hypothesised that the NRR follows a Mars-van-Krevelen (MvK) mechanism on these catalyst surfaces. A MvK mechanism is characterised by the participation and incorporation of surface atoms in the reaction and product, which are replenished subsequently, concluding the catalytic cycle.[7] In case of the NRR, lattice nitrogen is directly protonated forming ammonia, which is released. The lattice nitrogen vacancy is replenished by gaseous nitrogen. The assumption is that replenishment of these lattice nitrogen vacancies, either as monomer or dimer, is energetically favourable compared to the sole adsorption of nitrogen on the surface of catalysts following the associative Heyrovsky-mechanism.[6] Therefore, TMN NRR catalysts should be more selective and active in theory. However, the primary competing HER reaction has a similar theoretical onset potential as the NRR and is kinetically favoured.

The electrochemical behaviour of selected synthesised zirconium nitride materials was exemplarily investigated to qualitatively deduce potential activity for the electrochemical NRR. A quantitative investigation of the electrochemical NRR activity, following current state-of-the-art protocol including ammonia quantification after prolonged turnover experiments and isotope-labelled experiments, was not within the scope of this work.[5] Instead of this conducted potentiodynamic experiments give insights to the general electrochemical behaviour and possible contributions of the material's NRR activity to the measured HER current density. These results are important prerequisite for subsequent quantitative investigations in the future, demonstrating their NRR potential, but can up to here not answer if a material is active for the NRR or not. To this end, cyclic voltammograms (CV) and linear sweep voltammograms (LSV) in argon, inert to NRR, and nitrogen, educt gas, were performed in a relevant potential region. All potentials are in reference to the used reversible hydrogen electrode (RHE). The upper potential was limited to +0.6 V vs. RHE in all measurements, which corresponds approximately to the initial open circuit potential, to avoid potential oxidation of the nitride material. Electrochemical (EC) cleaning of nitride catalysts has been described in literature to remove the surface oxide layer prior to investigations of the potential NRR activity.[8] EC cleaning was performed, because the synthesised materials showed a surface oxide layer as determined by XPS. EC cleaning was done by performing several fast CV scans (250 mV s^{-1}, ~100 cycles) in argon-saturated electrolyte and supplying the GDE with inert argon gas as well. Figure 8 illustrates the effect of the EC cleaning, showing the initial state before the cleaning (red line) and, in comparison, the steady state after cleaning (blue line). The reductive currents at low (more negative) potentials are related to the occurring HER, with a maximum of −2 mA cm^{-2} at −0.6 V in the initial state. No further pronounced signals are visible besides a small hump at ~0.0 V in the cathodic and at ~0.2 V in anodic potential scan, respectively. The EC cleaning resulted in an increased HER onset potential, generally narrowed HER region (see arrows in Fig-

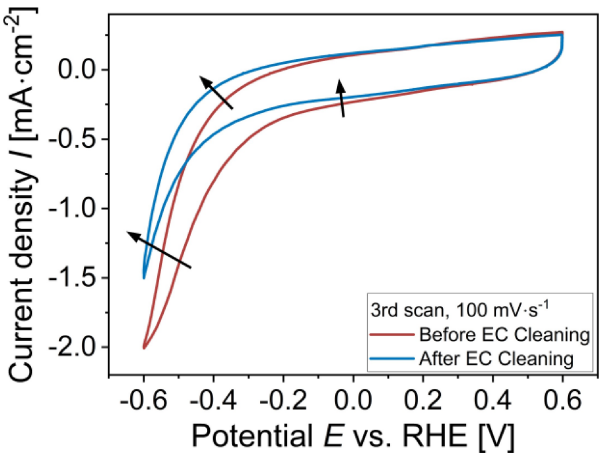

Figure 8. Electrochemical cleaning of ZrN-GDE (UGM 1150 °C, *Ca0.5*) in 0.1 M sulfuric acid electrolyte: Cyclic voltammetry (100 mV s^{-1}) in argon-fed electrolyte before (red line) and after electrochemical (EC) cleaning (blue line).

ure 8) and a lower maximum reductive current of −1.5 mA cm^{-2}, indicating a diminished HER activity with consecutive scans. There is no significant change between scans after EC cleaning in the positive potential region from 0 V to the chosen upper limit of +0.6 V, showing a stable state. The continuous reduction of the surface oxide species during the EC cleaning seems to have reduced the HER activity, explaining the observed quickly-diminished reductive currents within the initial consecutive scans. Furthermore, NRR should initially occur in inert argon gas, due to the assumed MvK mechanism, until active lattice nitrogen is depleted, as there is no nitrogen gas supplied for replenishment. To qualitatively deduce potential activity for the electrochemical NRR, CV and LSV analysis were compared by supplying reactive nitrogen to the GDE in separate measurements of the same sample, while the electrolyte was furthermore saturated with argon (Figure 9). Only the backwards scan of the third cycle of each CV is shown for the sake of clarity.

The first material, 1150 °C *Ca0.5* (Figure 9a and d), was chosen for its high nitride and phase purity, low residual carbon content and high crystallinity. The material pyrolyzed at 900 °C with a calcium admixture *of Ca0.5* (Figure 9b and e) was chosen in comparison, because it contains more minor phase, is less crystalline and contains more residual carbon. The last chosen material was pyrolyzed at 900 °C, but had the highest calcium admixture of *Ca2.0*. This material consists mainly of oxynitride phases and likely contains the least amount of carbon. The generally observed behaviour will be exemplarily described for the first measured sample of the 1150 °C *Ca0.5* material (Figure 9d, GDE–A). The maximum reductive current was about −3.5 mA cm^{-1} in inert argon (red line) after EC cleaning. This current is likely caused solely by HER as discussed before. Switching the supplied gas to reactive nitrogen (blue line), the reductive current increased to approximately −7 mA cm^{-2}, which is on the order of magnitude seen before. In addition, there was a crossover of currents at approximately −0.3 V in the complete CVs (not shown). This current crossover, a higher current at the same potential in the anodic scan than the cathodic scan, is characteristic for a higher activity of the reduced state than the oxidised state for both measurements. An electrochemical NRR occurring simultaneously to the HER supplying reactive nitrogen can explain the lower onset potential and increased reductive currents compared to inert argon. A similar behaviour was observed by Hanifpour et al. investigating a polycrystalline ZrN film and other TMNs.[8,46–48] A higher reductive current in reactive nitrogen than inert argon was observed for all tested samples and materials. The 900 °C samples with *Ca0.5* and *Ca2.0*, which contain oxynitrides to differing amounts, showed higher current density in LSV

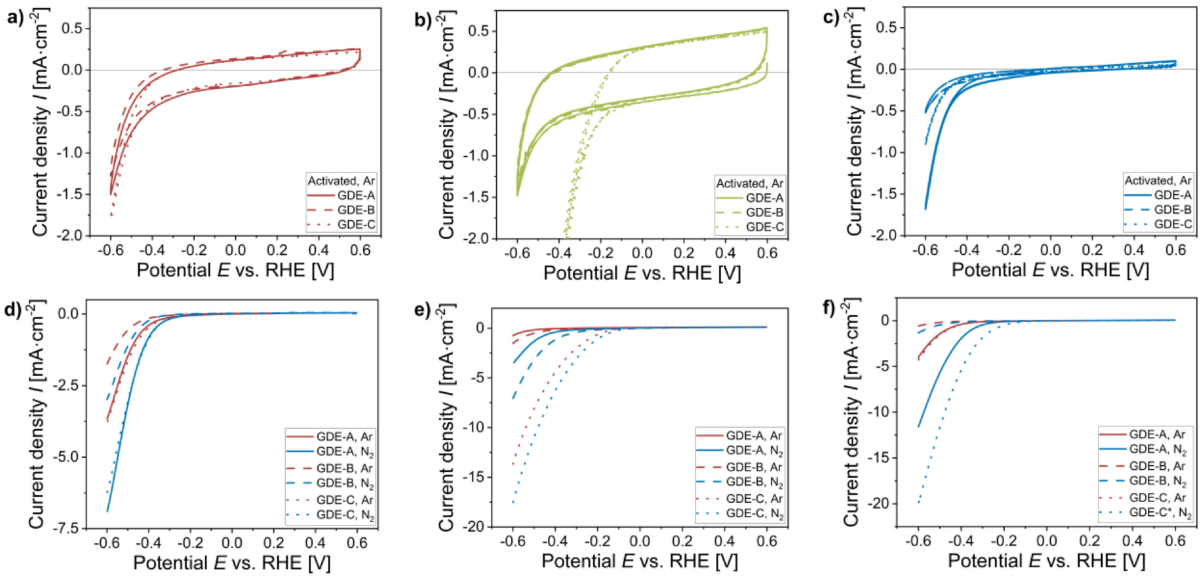

Figure 9. Electrochemical characterization of GDEs of selected synthesized zirconium nitride materials. The top row shows the CVs in argon after activation: (a) 1150 °C, *Ca0.5*, (b) 900 °C, *Ca0.5*, (c) 900 °C, *Ca2.0*. The bottom row shows the material behavior in argon (red) and nitrogen (blue) as qualitative comparative measure of the NRR activity: (d) 1150 °C, *Ca0.5*, (e) 900 °C, *Ca0.5*, (f) 900 °C, *Ca2.0*.

investigation (Figure 9e and f). Speculatively, oxygen neighbouring nitrogen atoms or vacancies in the nitride lattice could influence single mechanistic reaction steps resulting in an energetically beneficial NRR via MvK, which was postulated for vanadium oxynitride in literature.[49] However, there is a large variance within and between materials. The current increased on average by 75 ± 13 %, 252 ± 194 % and 228 ± 120 % for the three materials. This increase in current is substantial and promising if it is caused by NRR. Still, further understanding of the material, reaction and electrochemical system is required, especially in light of the different EC behaviour of one sample to the next within one batch.

Furthermore, this qualitative comparison of reductive currents is limited in its significance. A proof of genuine electrochemical NRR to date requires a quantitative determination of formed ammonia by trace analysis, as well as isotope-labelled experiments, proving the supplied gas as nitrogen source of the ammonia, which is both beyond the scope of this study. In addition, further pursuit of robust electrochemical protocols that avoid false positive results due to contaminations and other effects is required.[5,50] Moreover, TMN are also discussed to undergo non-catalytic decomposition resulting in ammonia formation instead of genuine NRR.[51] Thus, the state-of-the-art experimental data on genuine NRR activity of TMNs is as yet inconclusive, but they remain promising due to the great catalytic potential for the NRR via the MvK mechanism.[52] Consequently, the theoretically predicted activity and onset potential for ZrN, depending on crystal structure and facet, are yet to be confirmed in literature.[7] More in-depth electrochemical characterisation coupled with quantitative trace analysis of the electrolyte (and gases) for ammonia is needed to further understand and elucidate possible discrepancies between theory and practice, which will be the scope of further studies. Equally important, reproduction and reproducibility of determined NRR activity must be a cornerstone of the continued electrochemical NRR research, especially on TMNs. The synthesised ZrN materials are interesting, but remain to be proven active for a catalytic electrochemical ammonia production.

3. Discussion

3.1. Zirconium Nitride Synthesis

The UGM allows for easy and accessible synthesis of nanoparticulate ZrN at moderate temperatures. The formation of zirconium nitride requires a minimum pyrolysis temperature of 900 °C (literature ≈840 °C) to form from an intermediate oxynitride phase (Figure 1).[9] Oxide and oxynitride phases occur alongside the desired ZrN depending on the composition and pyrolysis conditions i.e. pyrolysis temperature (Figure 1), calcium admixture (Figure 2), urea content (Figures S9–S11) and pyrolysis crucible (Figures S12–S15). Presumably, amorphous zirconium dioxide is progressively nitrided by reactive nitrogen species, which are generated during the decomposition of urea. This conversion results in oxynitrides with increasing nitrogen content (β′, β, γ). The irreversible decomposition of this nitrogen-rich oxynitride γ-phase yields nitride and a less nitrogen-rich oxynitride following the quasi-binary phase diagram determined by M. Lerch et al.[9] This resulting oxynitride is in turn nitrided under the right conditions, until it also decomposes into nitride and oxynitride. This cycle continues until the nitridation reaction ceases or the oxide has been completely converted. This process explains the observed minor and major oxide and oxynitride phases and their trends with added calcium ions (Figure 2), which slows urea decomposition.[15] Urea decomposition must generate a critical local concentration of reactive nitrogen species for nitride to occur, which was shown by the occurrence of nitride at the lower urea content of U5. Nitride did form, but only as a minor phase (Figure S9). Moreover, this nitriding atmosphere must be sufficient in concentration over time, the generation neither too fast nor too slow for extensive conversion. A small calcium admixture results in a higher average concentration in time, reducing the loss of reactive nitrogen species, resulting in more extensive conversion to the nitride. Already-formed particles grow for a longer time, forming larger more crystalline particles. A large calcium admixture slows the generation of reactive nitrogen species so much that the necessary critical concentration is not reached locally. No nitride, and only less nitrogen-rich oxynitrides, form in consequence, depending on the magnitude of calcium admixture (Figure 2). The beneficial effect of using crucibles with a closed lid works in the same way as a slightly-slowed urea decomposition. The lid retains the nitriding atmosphere for a longer time, resulting in more nitride-formation by better utilisation of the atmosphere (Figure S13). A pyrolysis temperature above 900 °C also has a beneficial effect on the conversion of the oxide to the desired nitride, due to two effects. The first effect is a different decomposition path of the γ-phase. The γ-phase decomposes to nitride, nitrogen and oxide rather than oxynitride above approximately 1000 °C, following the quasi-binary phase diagram of M. Lerch (Equation (4)).[9] The theoretical yield is larger by a third, again assuming a stoichiometric decomposition (Equation (5)). The other effect at an even higher temperature of 1400 °C is the partial nitridation of zirconium dioxide directly by the nitrogen atmosphere.[26] This source of nitrogen is continuous over time, assisting the synthesis by the UGM. However, the improved diffusion rates at elevated temperatures must not be disregarded. The possibility of directly (partially) nitriding zirconium dioxide by nitrogen at temperature of ≥1400 °C also enables the carbothermal nitridation (CN), which then becomes an alternative synthesis route.

$$4\ Zr_2ON_2 \rightarrow 2\ ZrO_2 + 6\ ZrN + \ N_2 \tag{4}$$

$$\frac{6\ M_{ZrN}}{6\ M_{ZrN} + 2\ M_{ZrO_2}} = \frac{6 \cdot 105.2307}{6 \cdot 105.2307 + 2 \cdot 123.222} \approx 72\,\% \tag{5}$$

Carbothermal nitridation of zirconium was successful at a temperature of 1400 °C in nitrogen using a molar ratio of carbon black to zirconium dioxide of 4. A significant amount of ZrC determined by Vegard's Law ($ZrN_{0.63\pm0.17}C_{0.37\pm0.17}$) remained

at a dwelling time of 3 hours. Zirconium carbide is an intermediate phase in the carbothermal nitridation of zirconium.[37] This undesired phase was greatly reduced by increasing the dwelling time to 4.5 hours ($ZrN_{0.90\pm0.05}C_{0.10\pm0.05}$), which confirms it is indeed an intermediate to the nitride. Adding carbon in excess of 4 to the theoretical molar ratio of 2 (Equation (3)) caused undesired carbon black to remain in the product with a mass fraction of roughly 16 to 20% (Table 2). This corresponds to approximately half of the carbon added to the zirconium dioxide, indicating that the theoretical molar ratio of 2 should suffice. A molar ratio of 2 at a dwelling time of 4.5 hours consequently resulted ZrN ($ZrN_{0.91\pm0.05}C_{0.09\pm0.05}$) free of residual carbon, albeit with a minor zirconium dioxide fraction. A slight adjustment of the carbon ratio above 2 could lead to phase-pure ZrN without residual carbon.

Comparing the synthesised material properties to literature is hampered by differing synthesis routes, different synthesis conditions, choice of suitable comparator and available literature. However, Das et al. used a synthesis route that slots in between UGM and CN by directly pyrolyzing mixtures of zirconium tetrachloride and urea at high temperature and evaluating the nitride stoichiometry by Vegard's Law as well.[35] They found trends in occurring phases and nitride purity which match our own observations. A sole major zirconium nitride phase contains some carbon as zirconium carbide in the crystal lattice as determined by Vegard's law. The achieved stoichiometry of $ZrN_{0.91}C_{0.09}$ at 1400 °C by Das et al. fits our findings well, although derived by use of different reference lattice constants. An occurring minor nitride phase alongside other major phases is purer than a (sole) major nitride phase. Both a critical urea content and pyrolysis temperature are required for nitride to form. The minor phases consist of tetragonal and monoclinic zirconium dioxide. The higher the pyrolysis temperature, the more carbide forms. They also found similar amounts of residual carbon remaining in the product, which is located around nitride particles in TEM images. Overall, the material properties are comparable, although the synthesis routes differ greatly.

3.2. Comparison of Synthesis Routes

Both synthesis routes, UGM and CN, are successful in synthesising nanoparticulate zirconium nitride with certain advantages and disadvantages. UGM enables a synthesis of zirconium nitride starting at a moderate temperature of 900 °C using cheap, safe to handle, non-toxic urea. The method also allows to synthesise γ-phase oxynitride by adjusting process parameters. However, a high urea content is necessary for high nitride yield, leading to a small absolute yield and undesired residual carbon in the pyrolysis product. Residual minor phases are a complex, likely oxide-oxynitride mixture. A small calcium admixture improves the synthesis. It reduces the amount of minor phase and residual carbon as well as improving crystallinity. Having said this, the admixture requires sample purification, while some calcium likely remains in the sample. The higher crystallinity is a consequence of likely larger particles, which is undesired. Similarly, the use of zirconium tetrachloride as zirconium precursor results in some residual chloride. Higher pyrolysis temperatures reduce minor phases as well, but decrease nitride purity, increase ZrC incorporation, and CN becomes a feasible alternative method at high temperatures (≥1400 °C). Synthesising high-purity ZrN without any minor phases or residual carbon may not be possible using UGM alone. CN enables synthesising zirconium nitride at 1400 °C in a nitrogen atmosphere using readily available nanoparticulate zirconium dioxide and a suitable carbon source such as carbon black. Tuning the amount of added carbon as oxygen getter and dwelling time might enable a synthesis of pure ZrN without either minor phase or residual carbon. However, the required high temperature, and reaction mechanism, likely results in larger nanoparticles and a slightly lower purity than using UGM.

Optimising the zirconium nitride synthesis for high purity of the nitride, phases and product generally has the same constraints for both used methods, a perfectly pure nitride was hitherto not achievable in this work without any minor phases or some residual carbon. Further optimisation will be carried out to this end.

4. Conclusions

The urea-glass method (UGM) was systematically investigated in this study as a simple and accessible synthesise route for nanoparticulate zirconium nitride (ZrN) for the prospective use as an electrocatalyst. The synthesis of ZrN by UGM follows the quasi-binary phase diagram of ZrO_2–Zr_3N_4, occurring via irreversible decomposition of the γ-phase oxynitride Zr_2ON_2 starting above 800 °C. An increased pyrolysis temperature reduces the amount of minor phase, but results in reduced nitride purity and likely larger particle size. Addition of calcium ions affects the urea decomposition, improving the nitride conversion in small amounts, reducing the amount of residual carbon and improving crystallinity, but likely due to larger particles. A simple carbothermal nitridation (CN) of commercial nanoparticulate zirconium dioxide with carbon black was successfully used in comparison to UGM. An adjusted pyrolysis composition resulted in nanoparticulate ZrN of similar purity without residual carbon, but with some remaining minor oxide phase. Regardless of the synthesis method, an increased synthesis temperature reduces the amount of minor phase but increases the particle size and seems to be accompanied by lower nitride purity. Both synthesis methods resulted in similarly pure nitrides but the utilized analysis methods are insufficient to exhaustively determine the material composition in regard to the elemental composition, as nitrides are easily contaminated by carbon and oxygen. An elemental analysis suitable for these refractory materials is needed to determine the absolute content of nitrogen, oxygen and carbon to account for their effect. The initial qualitative investigation of the ZrN nanoparticles synthesized by UGM for NRR was promising, there is substantially higher reductive current in nitrogen than argon, but further quantitative measurements of the electrochemically-produced ammonia must follow.

Methods

Synthesis – Urea-Glass Method (UGM)

Zirconium tetrachloride (ABCR, AB122360, 99.5% Zr) powder is weighed into a three-neck round-bottom flask in a glovebox. The sealed flask is transferred to a Schlenk line. Dried ethanol (Sigma-Aldrich, 24102, 99.8%) is added (45 mL g^{-1}_{ZrCl4}) and stirred at room temperature until complete dissolution of the powder.[23] Then urea (Sigma-Aldrich, 33247–250G, $\geq$99.5%) is added to the solution in a set molar ratio to the zirconium of 5 or 15 (U5, U15). The urea containing solution was stirred for 2 h to allow sufficient time for dissolution and complexation. Calcium chloride dihydrate (Sigma-Aldrich, 223506, $\geq$99%) is added in a set molar ratio to the zirconium tetrachloride (*Ca0.25*, *Ca0.5*, *Ca1.0*, *Ca2.0*) after complete dissolution of the added urea. This admixture of calcium chloride dihydrate is simply referred to as 'calcium admixture' in the main text. The formed solution is transparent, colourless and slightly hazy. The final step is addition of 28 wt.% ammonium hydroxide solution (Alfa Aesar, L13168, 28 wt.%) (2.1 mL g^{-1}_{ZrCl4}) to induce rapid crosslinking. The pulpy mixture is spread in a crystallization bowl and dried over night at 60 °C. The dry mixture is scraped out of the bowl and squashed into a fine, white, pourable powder. This powdery pyrolysis mixture is stored in closed rolled-rim glass vials until use.

Pyrolysis – UGM

The UGM pyrolysis mixture is poured into a crucible (glazed or unglazed alumina boat, glassy carbon crucible, with or without lid) and placed in a tube furnace (Nabertherm, RHTC 80–230/15, alumina tube C799, alumina 99.7%, max. 1500 °C). Nitrogen (Linde, 5.0) is flushed through the tube at 100 L min^{-1} (NTP) for 15 min before the oven program is started. The sample is heated at 5 °C min^{-1} to the final pyrolysis temperature (800, 900, 1150, 1400 °C) and kept there for the set dwelling time (2, 3, 4.5 h). The cooling rate is 5 °C min^{-1} until limited by natural cooling at lower temperatures. The sample is left in the oven until room temperature has been reached, only then the gas flow is switched off.

The pyrolysis product is scraped from the crucible and ground by hand to a fine powder. This powder is washed with 10 mL of 1 M hydrochloric acid in a 15 mL centrifuge tube using a roll mixer for 5 to 6 h to remove residual calcium species. The powder is separated by centrifugation and washed three times with ultrapure water, supernatant is decanted. Residual liquid is removed by drying at 60 °C overnight. This powder is used without further purification.

High-Temperature Synthesis – Carbothermal nitridation (CN)

Commercial nanoparticulate zirconium dioxide i.e. zirconia powder (Sigma-Aldrich, 544760–5G, Zirconium(IV)oxide, nanopowder, $<$60 nm particle size (TEM)) is weighed into a rolled rim glass vial. Carbon black (Cabot, VULCAN® XC72) is added in a molar ratio to the zirconium of 2 or 4. Three zirconia grinding balls (5 mm diameter) are added and the mixture is homogenized overnight using a roll mixer. The homogenized powder is used as pyrolysis mixture after removal of the zirconia grinding balls.

The pyrolysis mixture is transferred into a glassy carbon (GC) crucible on which a GC plate is placed as lid. The crucible is placed into the high temperature oven (Carbolite Gero, LHTG 100–200/30, max. 3000 °C). The oven is heated at 10 °C min^{-1} to 1400 °C under a nitrogen gas flow of 150 L h^{-1} (NTP) and kept there for a set dwelling time (3, 4.5 h) under a nitrogen gas flow of 200 L h^{-1} (NTP). The sample cooled down to room temperature with 10 °C min^{-1} under this atmosphere.

Thermogravimetric Analysis (TGA)

Thermogravimetric analysis (TGA) was performed using a PerkinElmer TGA4000 with 180 µL aluminium oxide crucibles using either a nitrogen (Linde, 5.0) or oxygen (Linde 6.0) gas flow of 40 mL min^{-1}. The temperature programme is given in the supporting information (SI S4, S10).

X-ray Diffraction (XRD)

Powder X-ray diffraction (XRD) measurements were performed on a Malvern Panalytical Empyrean Series 2 diffractometer in Bragg-Brentano configuration with a Cu X-ray tube and Pixcel1D detector (240 mm, Soller slits 0.04 rad, divergence slit 1/8°, anti-scatter slit 1/2°, PIXcel1D-Medipix 3 with FASS, Cu $K\alpha_1$ 0.1540980 nm, anti-scatter slit AS slit 7.5 mm, 40 kV, 40 mA). Samples were measured as coating on circular glass slides (32 mm diameter, 3 mm thickness) if not specified differently. To this end, 20 mg of powder was dispersed in 200 µL isopropanol using an ultrasonic bath. The whole volume was aspirated using an Eppendorf pipette and drop-cast onto the centre of the glass slide. The coating was left to dry at room temperature. Diffractograms were recorded from 10° to 90° 2θ in 0.013° steps with an accumulation time of 800 s per step spinning at 2 U s^{-1} if not specified differently (total time per sample 5 h). The general aim was to achieve $\geq$50.000 counts for peaks with $\geq$50% intensity and $\geq$5.000 counts for peaks of $\geq$5% intensity inspired by the recommendations of the International Centre for Diffraction Data (ICDD).

Transmission Electron Microscopy (TEM)

Samples were prepared using TEM grids (Plano, TEM SF 162, HR-TEM S 162) with a carbon and, in case of HR-TEM, formvar coating. 1 mg of sample powder was dispersed in 4 mL ethanol absolute using an ultrasonic bath. 8 µL of homogeneous dispersion was dropped onto a grid and dried at room temperature. TEM measurements were conducted using a Zeiss EM902 A with tungsten electrode at an acceleration voltage of 80 kV. High resolution (HR) TEM measurements were performed using a Joel JEM2100 F with a Schottky-emitter at an acceleration voltage of 200 kV. Energy-dispersive X-ray spectroscopy (EDS) was done using an Oxford INCA Energy TEM250 EDS-system with a silicon drift X-ray detector MAX80.

X-ray Photoelectron Spectroscopy (XPS)

X-ray photoelectron spectroscopy (XPS) was performed using a Thermo Fisher Scientific ESCALAB 250Xi with monochromatic Al Kα photon radiation ($h\nu$ = 1486.6 eV). Pristine powder samples were pressed into the cavity of an aluminium sample holder. Survey scans were collected in triplicate (100 eV, 1 eV step size, 10 ms). High resolution spectra of Zr 3d, N 1s, O 1s and C 1s were collected separately (10 eV, 0.02 eV step size, 50 ms) with 5 scans per Element with exception of N, for which 10 scans performed. The flood gun was used to compensate charging effects of potentially oxidized surfaces. Samples were measured without prior sputter-cleaning. All spectra were charge corrected to the aliphatic carbon signals (component c1 in respective C 1s spectra) at a binding energy of 248.8 eV. Peak deconvolution analysis was performed by a product of Gaussian and Lorentzian Peak shapes with a Shirley background using the Avantage software (version 5.9925).

Electrochemical Analysis (EC)

Electrochemical analysis was performed using a commercial Gaskatel FlexCell-PTFE (SKU: 83100) measurement half-cell. A classical three-electrode setup was employed using self-made gas diffusion electrodes (GDE) as working electrode. GDEs of ZrN material (U15, *Ca0.5*, 1150 °C ()) were spray-coated by hand using a professional airbrush-pistol. A measured amount of ink (isopropyl alcohol, ultrapure water, 1:1 V:V) was deposited on a vertically fixed piece of gas diffusion layer (9×9 $cm^{[2]}$) using a mask leaving an area of 6×6 $cm^{[2]}$ uncovered. Target loading was 1 mg cm^{-2} catalyst material with 30 wt.% Nafion in the coating. More details regarding the manual spray-coating and electrochemical setup are available in the supporting information of a prior publication.[53] A PtIr-spiral supplied with the cell was used as counter electrode. The reference electrode consisted of a Gaskatel Mini-HydroFlex (SKU: 81020) reversible hydrogen electrode (RHE). All potentials are reported versus RHE scale. The experiments were controlled by a Metrohm Autolab PG128 potentiostat using the manufacturer supplied Nova® software version 2.1. The electrolyte consisted of 0.1 molar high-purity sulfuric acid (Merck, 1.01516.0250, sulfuric acid 96%, ultrapure) freshly prepared. The supplied N2 and Ar gases were purged through 5 mM sulfuric acid electrolyte and ultrapure water as basic cleaning step for potential NH_3 contaminations before entering the electrochemical cell. The experiments were performed at room temperature.

The electrochemical test protocol consists of (1) cyclic voltammetry (CV) measurements with a scan rate of 100 mV s^{-1}, (2) electrochemical (EC) cleaning by several fast CV cycles (250 mV s^{-1}, ~100 scans), (3) CV measurements (100 mV s^{-1}), (4) double layer capacitance measurements and (5) slow CV measurements (10 mV s^{-1}). The double layer capacitance measurements were performed in faradaic current regime by CV. It was recorded at + 0.2 V in a small potential window (± 0.1 V) at several scan rates (500, 200, 100, 50, 20, 10 mV s^{-1}). The initial measurement sequence (1–5) was performed in Ar-saturated electrolyte to evaluate the electrochemical background signal. This was followed by repeating steps (3) and (5) in N_2-saturated electrolyte to evaluate potentially increased currents due to ongoing NRR in addition to background HER. Thus, potential NRR activity is qualitatively investigated as initial step of a more sophisticated testing protocol, which is required to prove genuine NRR activity and is beyond the scope of this study.

Supporting Information Summary

Supporting information is available from the Wiley Online Library or from the author.

Acknowledgements

This work was partially funded by the German Research Foundation (Deutsche Forschungsgemeinschaft, DFG) priority programme 2370, Project SUNRed (project number 460921994).

The powder X-ray diffraction and X-ray photoelectron spectroscopy measurements were made possible by DFG funding through grant number 276839650 and 251668893 respectively. Furthermore, the authors thank Prof. Wittstock for access to the X-ray photoelectron spectrometer.

The authors acknowledge the Electron and Light Microscopy Service Unit, Carl von Ossietzky University of Oldenburg, for the use of the imaging facilities. The authors further thank Heinrich Vocke (Carl von Ossietzky University of Oldenburg) for conducting HR-TEM measurements and Jasmin Schmeling (DLR) for conducting TEM measurements as well as evaluation of the SAED images. The authors also thank Jana Ewert for her assistance in operating and using the high temperature oven. Open Access funding enabled and organized by Projekt DEAL.

Conflict of Interests

The authors declare no conflict of interest.

Data Availability Statement

The data that support the findings of this study are available from the corresponding author upon reasonable request.

Keywords: Transition metal nitride · Zirconium nitrides · Nanoparticles · Calcium-assisted urea-glass method · Carbothermal nitridation · Gas diffusion electrodes · Electrochemical ammonia synthesis

[1] R. Schlögl, in *The Chemistry and Physics of Solid Surfaces and Heterogeneous Catalysis* (Ed: J. R. Jennings), Springer Germany, **1995**.
[2] L. E. Apodaca, *Nitrogen (FIXED)–Ammonia, in Mineral Commodity Summaries*, U.S. Department of the Interior, U.S. Geological Survey, **2022**, DOI: 10.3133/mcs2022.
[3] D. J. Ham, J. S. Lee, *Energies (Basel, Switz.)* **2009**, *2*(4), 873–899.
[4] H. Wang, J. Li, K. Li, Y. Lin, J. Chen, L. Gao, V. Nicolosi, X. Xiao, J.-M. Lee, *Chem. Soc. Rev.* **2021**, *50*(2), 1354–1390.
[5] H. Iriawan, S. Z. Andersen, X. Zhang, B. M. Comer, J. Barrio, P. Chen, A. J. Medford, I. E. L. Stephens, I. Chorkendorff, Y. Shao-Horn, *Nat. Rev. Methods Primers* **2021**, *1*(1), 56.
[6] J. H. Montoya, C. Tsai, A. Vojvodic, J. K. Norskov, *ChemSusChem* **2015**, *8*(13), 2180–2186.
[7] Y. Abghoui, A. L. Garden, J. G. Howalt, T. Vegge, E. Skúlason, *ACS Catal.* **2015**, *6*(2), 635–646.
[8] F. Hanifpour, C. P. Canales, E. G. Fridriksson, A. Sveinbjörnsson, T. K. Tryggvason, J. Yang, C. Arthur, S. Jónsdóttir, A. L. Garden, S. Ólafsson, K. Leósson, L. Árnadóttir, E. Lewin, Y. Abghoui, Á. S. Ingason, F. Magnus, H. D. Flosadóttir, E. Skúlason, *J. Catal.* **2022**, *413*, 956–967.
[9] M. Lerch, *J. Mater. Sci. Lett.* **1998**, *17*(6), 441–443.
[10] M. Banerjee, N. B. Srinivasan, H. Zhu, S. J. Kim, K. Xu, M. Winter, H.-W. Becker, D. Rogalla, T. de los Arcos, D. Bekermann, D. Barreca, R. A. Fischer, A. Devi, *Cryst. Growth Des.* **2012**, *12*(10), 5079–5089.
[11] H. Yamamura, S. Emoto, T. Mori, *J. Ceram. Soc. Japan* **1998**, *106*(1235), 650–653.
[12] S. Zhao, J. Ma, R. Xu, X. Lin, X. Cheng, S. Hao, X. Zhao, C. Deng, B. Liu, *Sci Rep.* **2019**, *9*(1), 19199.
[13] A. J. Parkison, A. T. Nelson, *J. Am. Ceram. Soc.* **2016**, *99*(5), 1525–1533.
[14] C. Giordano, C. Erpen, W. Yao, B. Milke, M. Antonietti, *Chem. Mater.* **2009**, *21*(21), 5136–5144.
[15] Q. Gao, C. Giordano, M. Antonietti, *Small* **2011**, *7*(23), 3334–3340.
[16] M. Lerch, J. Wrba, *J. Mater. Sci. Lett.* **1996**, *15*(5), 378–380.
[17] K. Constant, R. Kieffer, P. Ettmayer, *Monatsh. Chem./Chemical Monthly* **1975**, *106*, 823–832.
[18] S. J. Clarke, C. W. Michie, M. J. Rosseinsky, *J. Solid State Chem.* **1999**, *146*(2), 399–405.
[19] T. Bredow, M. Lerch, *Z. Anorg. Allg. Chem.* **2007**, *633*(15), 2598–2602.
[20] T. Locherer, L. Dubrovinsky, H. Fuess, *Solid State Commun.* **2007**, *143*(8–9), 408–411.
[21] R. J. Hill, L. M. D. Cranswick, *J. Appl. Crystallogr.* **1994**, *27*(5), 802–844.
[22] J. Málek, L. Beneš, T. Mitsuhashi, *Powder Diffr.* **1997**, *12*(2), 96–98.
[23] D. B. Williams, M. Lawton, *J. Org. Chem.* **2010**, *75*(24), 4.

[24] R. C. Mehrotra, *Inorg. Chim. Acta, Rev.* **1967**, *1*, 99–112.
[25] R. Srinivasan, B. H. Davis, O. B. Cavin, C. R. Hubbard, *J. Am. Ceram. Soc.* **1992**, *75*(5), 1217–1222.
[26] M. Lerch, *J. Am. Ceram. Soc.* **1996**, *79*(10), 2641–2644.
[27] Y. Yuan, J. Wang, S. Adimi, H. Shen, T. Thomas, R. Ma, J. P. Attfield, M. Yang, *Nat. Mater.* **2019**, *19*(3), 282–286.
[28] R. Allmann, in *Powder Diffraction: Theory, Practice*, (Eds: R. E. Dinnebier, S. J. L. Billinge), RSC Publishing, UK, **2008**.
[29] A. A. M. Ali, M. I. Zaki, *Thermochim. Acta* **2002**, *387*(1), 29–38.
[30] J. Desmaison, *Nitrogen diffusion in zirconium nitride* (Doctoral dissertation), **1973** (https://scholar.google.com/scholar?hl=de&as_sdt=0%2C5&q=J.+Desmaison+1973&btnG=).
[31] M. Lerch, F. Krumeich, R. Hock, *Solid State Ion.* **1997**, *95*(1), 87–93.
[32] M. K. Motandi, Z. Zhang, S. Inkoua, L. Yan, *Environ. Prog. Sustainable Energy* **2022**, *41*(2), e13744.
[33] J. Qu, L. Sha, Z. Xu, Z. He, M. Wu, C. Wu, Q. Zhang, *Appl. Clay Sci.* **2019**, *173*, 29–34.
[34] M. Lerch, E. Füglein, J. Wrba, *Z. Anorg. Allg. Chem.* **1996**, *622*(2), 367–372.
[35] S. Das, D. Dubois, M. S. I. Sozal, Y. Emirov, B. Jafarizadeh, C. Wang, V. Drozd, A. Durygin, Z. Cheng, *J. Am. Ceram. Soc.* **2022**, *105*(6), 3925–3936.
[36] L. M. Berger, W. Gruner, E. Langholf, S. Stolle, *Int. J. Refract. Met. Hard Mater.* **1999**, *17*(1), 235–243.
[37] S. Zhao, R. Xu, J. Ma, C. Deng, X. Cheng, X. Zhao, S. Hao, J. Li, *Mater. Today Commun.* **2021**, *29*, 102968.
[38] G. Greczynski, D. Primetzhofer, J. Lu, L. Hultman, *Appl. Surf. Sci.* **2017**, *396*, 347–358.
[39] T. Muneshwar, K. Cadien, *Appl. Surf. Sci.* **2018**, *435*, 367–376.
[40] P. Prieto, L. Galán, J. M. Sanz, *Surf. Interface Anal.* **1994**, *21*(6–7), 395–399.
[41] M. Matsuoka, S. Isotani, W. Sucasaire, N. Kuratani, K. Ogata, *Surf. Coat. Technol.* **2008**, *202*(13), 3129–3135.
[42] I. Milošev, H. H. Strehblow, M. Gaberšček, B. Navinšek, *Surf. Interface Anal.* **1996**, *24*(7), 448–458.
[43] M. C. Biesinger, *Appl. Surf. Sci.* **2022**, *597*, 153681.
[44] I. Molodetsky, A. Navrotsky, F. DiSalvo, M. Lerch, *J. Mater. Res.* **2000**, *15*(11), 2558–2570.
[45] S. N. Katea, G. Westin, *Ceram. Int.* **2021**, *47*(8), 10828–10847.
[46] L. Zhang, X. Ji, X. Ren, Y. Luo, X. Shi, A. M. Asiri, B. Zheng, X. Sun, *ACS Sustainable Chem. Eng.* **2018**, *6*(8), 9550–9554.
[47] F. Hanifpour, C. P. Canales, E. G. Fridriksson, A. Sveinbjörnsson, T. K. Tryggvason, E. Lewin, F. Magnus, Á. S. Ingason, E. Skúlason, H. D. Flosadóttir, *Electrochim. Acta* **2022**, *403*, 139551.
[48] R. Zhang, Y. Zhang, X. Ren, G. Cui, A. M. Asiri, B. Zheng, X. Sun, *ACS Sustainable Chem. Eng.* **2018**, *6*(8), 9545–9549.
[49] X. Yang, S. Kattel, J. Nash, X. Chang, J. H. Lee, Y. Yan, J. G. Chen, B. Xu, *Angew. Chem., Int. Ed.* **2019**, *58*(39), 13768–13772.
[50] J. Choi, B. H. R. Suryanto, D. Wang, H.-L. Du, R. Y. Hodgetts, F. M. Ferrero Vallana, D. R. MacFarlane, A. N. Simonov, *Nat Commun.* **2020**, *11*(1), 5546.
[51] H.-L. Du, T. R. Gengenbach, R. Hodgetts, D. R. MacFarlane, A. N. Simonov, *ACS Sustainable Chem. Eng.* **2019**, *7*(7), 6839–6850.
[52] Z. Qiao, D. Johnson, A. Djire, *Science* **2021**, *2*(5), 100438.
[53] S. C. H. Bragulla, J. Lorenz, C. Harms, M. Wark, K. A. Friedrich, *ChemSusChem* **2023**, *16*(13), e202202211.

Manuscript received: April 19, 2024
Accepted manuscript online: June 20, 2024
Version of record online: ■■, ■■

RESEARCH ARTICLE

Zirconium nitride (ZrN) is a theoretically predicted active catalyst for the emerging electrochemical nitrogen reduction reaction (NRR). It can be synthesized by the urea-glass method (UGM) at moderate conditions. The Ca-assisted UGM is explored to improve the product purity of synthesized ZrN nanoparticles and test a selection thereof in qualitative electrochemical experiments for catalytic activity.

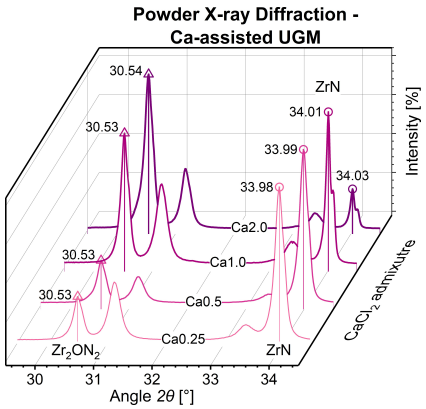

S. C. H. Bragulla, A. R. von Seggern, J. Lorenz, C. Harms, M. Wark, K. A. Friedrich**

1 – 20

Improving the Ca-assisted Urea-Glass Method for the Synthesis of Zirconium Nitride as Potential Electrocatalyst for the Nitrogen Reduction Reaction